The Titan Haze Simulation (THS) experiment on COSmIC. Part III. XANES study of laboratory analogs of Titan tholins

Michel Nuevo[1,2], Ella Sciamma-O'Brien[1], Scott A. Sandford[1], Farid Salama[1], Christopher K. Materese[3], and A.L. David Kilcoyne[4]

[1]NASA Ames Research Center, Space Science & Astrobiology Division, MS 245-6, Moffett Field, CA 94035, USA

[2]Bay Area Environmental Research Institute, NASA Research Park, MS 18-4, Moffett Field, CA 94035, USA

[3]NASA Goddard Space Flight Center, Code 691, Greenbelt, MD 20771, USA

[4]Advanced Light Source, Lawrence Berkeley National Laboratory, One Cyclotron Rd., Berkeley, CA 94720, USA

Submitted to Icarus, 29 July 2021

Reviewed (1), 7 September 2021

Revision (1) submitted, 13 October 2021

Reviewed (2), 9 November 2021

Revision (2) submitted, 3 December 2021

ABSTRACT

We have used the Titan Haze Simulation (THS) experimental set-up at NASA Ames' COSmIC facility to produce four laboratory analogs of Titan's aerosols, or tholins. These tholin samples were produced from four gas mixtures, representative of Titan's atmosphere, of initial compositions N_2:CH_4 (90:10 and 95:5) and N_2:CH_4:C_2H_2 (89.5:10:0.5 and 94.5:5:0.5) at 150 K, using a plasma discharge in the stream of a jet-cooled gas expansion. Here we present an ex-situ X-ray absorption near-edge structure (XANES) spectroscopy analysis of these four tholin samples. The C- and N-XANES spectra show the presence of various functional groups (aromatic carbon, imines, nitriles, etc.) whose abundances are correlated with (i) the relative proportions between N_2 and CH_4, and (ii) the presence or absence of C_2H_2 in the initial mixtures. In particular, mixtures containing C_2H_2 result in the formation of tholins consisting of more aromatic structures and displaying larger relative amounts of imines and nitriles, but lower overall nitrogen content. XANES spectroscopy also allowed for the determination of the elemental C/N ratios for the four tholins, which were all found to be low (< 2.5) and consistent with those measured for tholins produced in other, independent experimental set-ups. The C/N ratios of tholins produced from gas mixtures that contained C_2H_2 (2.2–2.4) were found to be about twice as large as those of tholins produced from gas mixtures that did not contain C_2H_2 (0.9–1.3). These new experimental results from the COSmIC/THS experiment demonstrate the impact initial precursors have on the nitrogen chemistry during the formation of tholins, which may help in the interpretation of observations and the development of models of Titan's atmosphere.

Keywords:

43 Titan, atmosphere

44 Tholins

45 Organic materials

46 XANES

47

48

1. Introduction

Titan, the largest moon of Saturn, is the only other object in the Solar System besides Earth that possesses a dense atmosphere (1.5 bar at the surface) whose composition is dominated by molecular nitrogen (N_2; 95–98%), with methane (CH_4; 2–5%) as the second most abundant gas (Hanel et al., 1981; Strobel and Shemansky, 1982; Lindal et al., 1983; Fulchignoni et al., 2005; Niemann et al., 2010). A complex organic chemistry between N_2 and CH_4, induced by solar ultraviolet (UV) photons and energetic particles, results in the formation of a large variety of organic compounds that include hydrocarbons such as acetylene (C_2H_2), ethylene (C_2H_4), ethane (C_2H_6), propyne (C_3H_4; also called methylacetylene), benzene (C_6H_6), nitriles such as hydrogen cyanide (HCN), hydrogen isocyanide (HNC), cyanoacetylene (HC_3N), acetonitrile (CH_3CN), ethyl cyanide (C_2H_5CN), and cyanogen (C_2N_2), as well as larger, more complex molecules that are believed to include aromatic and heteroaromatic compounds such as propane (C_3H_8), butane (C_4H_{10}), and polycyclic aromatic hydrocarbons (see Hörst, 2017; Barnes et al., 2021; and references therein for a complete review).

This complex organic chemistry taking place in the atmosphere also leads to the production of solid particles that form haze layers and play an important role in Titan's atmospheric dynamics, climate, as well as surface composition and processes. Because of its N_2-based dense atmosphere and its CH_4 cycle that resembles the hydrological cycle on Earth, Titan is often compared to the early Earth (Trainer et al., 2004; Lunine and Atreya, 2008; Roe, 2012; He and Smith, 2014). In recent years, Titan's atmosphere and surface were monitored in detail by the NASA *Cassini* mission, which orbited the Saturnian system from 2004 to 2017 (Matson et al., 2002, 2003;

Mitchell, 2006), as well as the ESA *Huygens* probe, which plunged into Titan's atmosphere and landed on its surface in 2005 (Lebretron et al., 2005; Owen, 2005; Zarnecki et al., 2005).

Many laboratory studies have simulated Titan's organic atmospheric chemistry in the past four decades, using various energy sources to induce the dissociation and ionization of N_2 and CH_4. These experiments result in the formation of refractory organic materials that are analogs of Titan's aerosols, often referred to as 'tholins' (Sagan and Khare, 1979; Cable et al., 2012; Coll et al., 2013; He et al., 2017; Hörst, 2017; Sciamma-O'Brien et al., 2017; Sebree et al., 2018). Tholins have been studied using a wide variety of techniques to determine their chemical compositions as well as their physical, chemical, and optical properties (e.g., Cable et al., 2012; Raulin et al., 2012; Brassé et al., 2015; Maillard et al., 2021; Schultz et al., 2021; and references therein). Among other findings, these studies have shown that tholins are macromolecular materials consisting mainly of carbon, nitrogen, and hydrogen, distributed among a mixture of aliphatic and aromatic structures.

In the present study, we produced tholins using the Titan Haze Simulation (THS) experimental set-up at NASA Ames' COsmic SImulation Chamber (COSmIC) facility from four initial gas mixtures that contained mainly N_2, together with 5% or 10% of CH_4, with or without the addition of 0.5% of C_2H_2 (see Section 2.1). We then analyzed these tholins ex situ using X-ray absorption near-edge structure (XANES) spectroscopy to obtain information on their chemical compositions and elemental C/N ratios. After describing the experimental protocol and analytical technique to produce and analyze our tholin samples, we compare our findings with those derived for tholins produced in other, independent experimental studies. Finally, we also describe how these new experimental results may have implications for the interpretation of observational data of Titan's atmosphere, especially during seasonal changes that result in the modification of the relative abundances of specific species.

2. Experimental Methods

2.1. Production of tholins with COSmIC/THS

Tholin samples were produced using the COSmIC/THS experimental set-up, whose mode of operation has been described in detail in previous publications (Sciamma-O'Brien et al., 2014, 2017; Salama et al., 2018). Briefly, a supersonic, adiabatic expansion is used to (i) cool down a gas mixture, flowing at 2,000 standard cubic centimeters per minute (sccm), to Titan-like temperatures (150 K), and (ii) decrease the gas pressure to 30 mbar (Broks et al., 2005; Biennier et al., 2006). A plasma discharge (typically, –700 to –1000 V) generated in the stream of that expansion is then used as an energy source to induce chemistry between the different molecular species present in the jet-cooled gas mixture (Sciamma-O'Brien et al., 2014), hence simulating the electron bombardment of Titan's atmosphere when passing through Saturn's magnetosphere. Although Titan's atmospheric chemistry is induced by both photolysis and radiolysis, it is experimentally advantageous to use a plasma discharge as the energy source instead of a UV lamp, as it allows to dissociate N_2, hence simulating the nitrogen chemistry taking place in Titan's atmosphere.

Resulting from this chemistry, larger species are formed in the gas phase, eventually leading to the formation of solid particles that can be jet-deposited onto substrates placed in the stream of the expansion. These solid particles, or tholins, are considered analogs of Titan's aerosols, which result from similar processes occurring in Titan's upper atmosphere. Figure 1 shows (a) a schematic of the pulsed discharge nozzle, which is at the core of the COSmIC/THS chamber and

117 is used to generate the pulsed planar plasma expansion (adapted from Broks et al., 2005), and (b)
118 a photograph of the COSmIC/THS pink N_2-based plasma expansion during solid sample
119 production (note: this picture shows an experiment in which a KBr window and two silicon wafers
120 placed 5 cm from the slit were used as substrates for the deposition). Previous studies have
121 demonstrated the effect of different gaseous precursors present in the initial gas mixture on the
122 formation of both gas-phase (Sciamma-O'Brien et al., 2014; Raymond et al., 2018) and solid-
123 phase (Sciamma-O'Brien et al., 2017) products in the COSmIC/THS chamber, particularly in the
124 cases where acetylene (C_2H_2) is added to N_2:CH_4 gas mixtures, which are traditionally used to
125 simulate Titan's atmospheric chemistry.

126 In the present study, tholins were produced from four different gas mixtures, namely,
127 N_2:CH_4 (90:10), N_2:CH_4:C_2H_2 (89.5:10:0.5), N_2:CH_4 (95:5), and N_2:CH_4:C_2H_2 (94.5:5:0.5). The
128 abundances of CH_4 relative to N_2 in the gas mixtures chosen for our experiments are representative
129 of the upper limit or higher than the relative CH_4 abundance observed with *Cassini* and *Huygens*
130 instruments as well as ground-based and space observatories (Hörst, 2017, and references therein).
131 Nevertheless, studying these gas mixtures present a couple of advantages: (i) these gas mixtures
132 have been used extensively in previous laboratory studies to simulate Titan's atmosphere, and the
133 results obtained here can therefore be compared with a large number of other experiments,
134 including those performed in our laboratory (Sciamma-O'Brien et al., 2014, 2017), and (ii) due to
135 the truncated chemistry occurring in our experimental set-up, starting with a higher relative
136 abundance of CH_4 allows for higher tholin production yield and therefore thicker samples, which
137 results in higher-quality analytical measurements. Finally, the purpose of adding 0.5% of C_2H_2 in
138 half of the gas mixtures is to study chemical processes which occur at later stages of the chemistry
139 that leads to the tholin formation in COSmIC, as the residence time of the gases in the chamber in

the plasma discharge is short and truncates the chemistry (see below). The addition of C_2H_2 also allowed us to compare our results with previous experiments (Sciamma-O'Brien et al., 2014, 2017).

The gas mixtures were introduced into the COSmIC chamber, exposed to a pulsed plasma discharge generated with a –800-V high voltage used as the energy source to induce the chemistry, and deposited for 1–2 hours (to ensure very little material was deposited; see Section **3.5**) onto silicon nitride (Si_3N_4) substrates placed 5 cm away from the slit, i.e., at the same distance as the substrates shown in Fig. 1(b). The voltage chosen for these experiments, which is higher than the voltage used in previous experiments (Sciamma-O'Brien et al., 2014, 2017), allowed for a higher production of grains in a shorter amount of time. **We expect the chemistry to be slightly different with –800 V than with –700 V, however, this does not impact the results of this study whose main goal is to compare 4 tholin samples produced under the same experimental conditions at –800 V.** The solid deposits were then collected in a glove box connected to the vacuum chamber and stored under an argon atmosphere in sealed containers with desiccant until further analysis. The four tholin samples were therefore exposed to air only at the time of their characterization by XANES spectroscopy, as described below.

2.2. XANES analysis of tholins

X-ray absorption near-edge structure (XANES) spectroscopy is a synchrotron-based soft X-ray micro-analytical technique that can be used to assess both the functional groups present in a sample and the relative elemental abundances between the elements studied. XANES spectroscopy at the carbon (C), nitrogen (N), and oxygen (O) 1s edges has been extensively used to study organic compounds in extraterrestrial samples such as meteorites, interplanetary dust particles (IDPs), and

cometary grains returned by the NASA Stardust mission (Bajt et al., 1996; Keller et al., 2004; Sandford et al., 2006; Cody et al., 2008; Wirick et al., 2009; Matrajt et al., 2010; De Gregorio et al., 2013). XANES spectroscopy has also been used to study laboratory refractory residues produced from the simultaneous deposition and UV irradiation of astrophysical ice mixture analogs (H_2O, CH_3OH, CO, NH_3, etc.) at low temperature (< 20 K) (Nuevo et al., 2011), as well as laboratory refractory organic materials produced from the UV irradiation or 1.2-keV electron bombardment of N_2:CH_4:CO (100:1:1) ice mixtures at 15 K, analog to the surface materials on Pluto and other trans-Neptunian objects (TNOs) and hereafter referred to as Pluto/TNO tholins (Materese et al., 2014, 2015). However, prior to this study, XANES spectroscopy analysis of Titan tholins has been reported only once for a sample produced from a N_2:CH_4 (95:5) gas mixture in another experimental set-up that uses a radiofrequency (RF) plasma to induce chemistry (Kuga et al., 2014). XANES spectroscopy is thus well suited for the study of the Titan tholins produced with COSmIC/THS, as the tholin production rate is extremely low in our experiments, which makes it difficult to use more commonly used combustion methods to obtain information on their elemental composition.

The tholin samples produced in this study were deposited on Si_3N_4 windows, which are suitable for XANES measurements. XANES measurements were conducted using the scanning transmission X-ray microscope (STXM) mounted on beamline 5.3.2.2 of the Advanced Light Source of the Lawrence Berkeley Laboratory. The STXM provides photons in the 250–700 eV range with a 10^7 photons s^{-1} flux (Kilcoyne et al., 2003). XANES spectra of the tholin samples were acquired in the 275–580 eV energy range in order to span the carbon (275–340 eV), nitrogen (385–440 eV), and oxygen (520–580 eV) 1s X-ray absorption edges, with an energy step size of 0.1 eV in the fine structure regions, and 1–2 eV in the pre- and post-edge regions (Cody et al.,

186 2008; Nuevo et al., 2011). All STXM data were reduced and analyzed using the aXis 2000
187 software.[1]

188 The C-, N-, and O-XANES spectra provided information on the functional groups present
189 in the tholin samples. In addition, the XANES spectra measured over the full 275–580 eV energy
190 range can be used to derive the relative elemental abundances between C, N, and O for each tholin
191 sample. This is done by computationally fitting the full-range XANES spectra of all tholins
192 spanning the C, N, and O 1s edges with the atomic mass absorption coefficients (Henke et al.,
193 1993) to estimate the overall increase in absorption above the ionization C, N, and O edges relative
194 to the absorption below these ionization edges. This is possible for low-*Z* elements, for which
195 absorption in the soft X-ray range is dominated by photo-ionization cross sections, and for which
196 atomic scattering is very weak (Stöhr, 1992). These abundances were then used to determine the
197 C/N and C/O ratios for each tholin sample, using the approach described in Cody et al. (2008) and
198 Nuevo et al. (2011).

199

200 **3. Results and Discussion**

201

202 *3.1. Carbon XANES spectra*

203

204 The normalized C-XANES spectra of all four tholins (Fig. 2) show the presence of a variety of
205 functional groups. **Table 1 lists t**he main **bands present in all tholin samples. They are**
206 **associated with** aromatic carbon (band C1 at ~285.2 eV), imines (C=N; band C2 at ~285.9 eV),
207 and nitriles (C≡N; band C3 at ~286.8 eV) (see Fig. 2 and Table 1). The relative proportions

[1] aXis 2000 is written in Interactive Data Language (IDL) and available for free for non-commercial use from http://unicorn.mcmaster.ca/aXis2000.html.

between these bands and the rest of the spectra vary significantly from one sample to another, although they appear to be more intense (relative to other bands) for tholins produced from the two gas mixtures containing acetylene (C_2H_2) (Fig. 2). Higher formation yields for aromatic compounds when acetylene is present are consistent with (i) previous mass spectrometry experiments conducted on COSmIC which showed that the addition of C_2H_2 in gas mixtures in which Ar or N_2 is the main component leads to the production of benzene in the gas phase (Contreras and Salama, 2013; Sciamma-O'Brien et al., 2014), and (ii) the fact that C_2H_2 is a known precursor of benzene in astrophysical environments (Frenklach and Feigelson, 1989; Cherchneff et al., 1992; Jäger et al., 2009; Zhao et al., 2016). Two other bands, assigned to amide groups and/or benzene (band C4 at 287.8–288.3 eV) and amorphous carbon, alcohols, and/or urea groups (band C5 at 288.9–289.7 eV), are also present in all tholins with varying intensities. Note that if a band is assigned to more than one functional group or structure, it may indicate the presence of either only one of these groups or several of them. In the case of the band C4, the presence of amide groups is supported by the band O3 (see Fig. S1 and Table S3 in the Supplementary Material). However, the contribution of benzene to this band, and thus its presence in the tholins, should not be ruled out, in particular in the tholins produced from the gas mixtures that contained acetylene, because acetylene is a well-known precursor to benzene (Frenklach and Feigelson, 1989; Cherchneff et al., 1992; Jäger et al., 2009; Zhao et al., 2016). Similarly, although the presence of alcohols and/or urea groups (band C5) is supported by the band O4 (alcohols) and a band at 532.1–532.2 eV (carboxyls) in Fig. S1 and Table S3, the presence of amorphous carbon should not be ruled out. The presence of O-bearing groups is believed to be mainly due to oxidation of the tholin samples when exposed to air during the transfer to the STXM vacuum chamber to conduct XANES

measurements, rather than from plasma-induced chemistry in the COSmIC/THS experiments, as discussed in more detail in Section **3.5.**

The C-XANES spectra of all four tholin samples also show the presence of multiple minor bands assigned to a wide variety of chemical functions (Table S1, Supplementary Material). Most of these assignments are tentative, as the intensities of most of these bands are small. Among these, bands at ~283, 284.6, ~286, and ~290.5 eV are associated with the presence of amorphous carbon (Table S1), which is mixed with aromatic carbon structures (band C1, 285.0–285.3 eV; Table 1) and aliphatic carbon chains (bands at ~287–288.5 eV; Table S1). The bands assigned to aliphatic carbon chains appear to be the strongest in the spectrum of the tholin sample produced from the N_2:CH_4 (90:10) mixture. A complete list of the bands observed in all four tholins is shown in Table S1. Other minor bands consistent with the presence of different types of aromatic materials are also observed in all tholins, including nitrogen-bearing heterocyclic compounds, but are stronger for tholins produced from mixtures containing C_2H_2; these bands are consistent with the presence of C- and N-bearing compounds similar to graphite (~285.2 and ~291.5 eV), pyridine (C_5H_5N; ~286.9 and ~290.6 eV), and fullerene (C_{60}; ~290.6 eV) (Table S1). However, it is difficult to estimate the relative intensities between aromatic hydrocarbons and heterocyclic aromatic hydrocarbons because most of these bands are weak and overlap with each other as well as with other bands.

The C-XANES spectra of both our N_2:CH_4 tholins (90:10 and 95:5) are consistent with the only other XANES study of a Titan tholin produced from a N_2:CH_4 (95:5) mixture in an RF plasma experimental set-up reported by Kuga et al. (2014). The two most intense bands observed in Kuga et al. (2014)'s C-XANES spectrum at 286.8 and 288.1 eV, assigned to nitriles/ketones and aliphatic carbon/amides, respectively, correspond to the bands C3 and C4 observed in our C-

XANES spectra (Fig. 2, Table 1). The C-XANES spectra of our four tholin samples also share strong similarities with those obtained in a XANES study of two laboratory-generated Pluto/TNO tholins produced from the UV photo-irradiation and 1.2-keV electron bombardment of N_2:CH_4:CO (100:1:1) ice mixtures (Materese et al., 2014, 2015). In particular, the C-XANES spectra of our four tholins and these two Pluto/TNO tholins show the presence of aromatic carbon (285.0–285.3 eV) and nitriles (399.3–400.0 eV).

3.2. Nitrogen XANES spectra

The normalized N-XANES spectra for all four of our tholin samples (Fig. 3) are consistent with their C-XANES spectra (Fig. 2, Section 3.1). **Table 1 lists t**he main bands observed **in all tholin samples. They** are associated with imines (band N1 at 398.9–399.2 eV in Fig. 3) and nitriles (band N2 at 399.8–400.0 eV), in particular for the tholins produced from mixtures containing **C_2H_2. In** the spectra of tholins produced from mixtures that did not contain acetylene, the band N2 is slightly redshifted (band N2* at 399.3–399.8 eV), indicating that the nitrile groups are mostly linked to aliphatic carbon chains (Pels et al., 1995; Shard et al., 2004; Ray et al., 2005; Leinweber et al., 2007; Cody et al., 2008), as opposed to nitrile groups linked to aromatic hydrocarbons (band N2) (Zhu et al., 1997). Another band (N3 at ~401.3 eV) that is observed in all spectra can be assigned to amino groups (Cody et al., 2011), although the position of this band is also consistent with the presence of amide groups (O=C–NH_x) and mirrors the presence of bands C4 in the C-XANES spectra (Fig. 2 and Table 1) and O3 in the O-XANES spectra (Fig. S1 and Table S3; Supplementary Material).

N-XANES spectra also contain several minor bands that are tentatively associated with a wide variety of functional groups or compounds (Table S2, Supplementary Material), including pyridine, pyrrole, different types of nitrogen heterocycles, nitroso groups, nitro groups, and oxidized variants of pyridine (pyridone and pyridine *N*-oxide). However, the assignments of these O-bearing species could not be confirmed by the presence of mirror bands in the O-XANES spectra (Table S3; Supplementary Material). Finally, multiple weak bands at ~400.5, ~401.3, and ~407.0 eV are consistent with the presence of nitrogen atoms inserted in graphene structures, supporting the bands associated with graphene-like structures in the C-XANES spectra (Section 3.1, Table S1).

As was the case for the C-XANES spectra, the N-XANES spectra of the four tholin samples studied here share similarities with the only other XANES spectrum of another Titan tholin sample produced from a N_2:CH_4 (95:5) gas mixture in a different experimental set-up (Kuga et al., 2014). In particular, the spectrum of our tholin sample produced from the N_2:CH_4 (95:5) gas mixture is very similar to that of Kuga et al. (2014), in which the two main bands observed at 398.9 and 399.7 eV, assigned to imines and nitriles, respectively, are comparable to the bands N1 and N2/N2* in our N-XANES spectra. The Pluto/TNO tholins reported by Materese et al. (2014, 2015) also share similarities with our tholin samples, with bands at 399.9 and 401.0 eV associated with nitriles and amides, respectively, comparable to the bands N2/N2* and N3 observed in our N-XANES spectra. In addition, although not explicitly reported in Materese et al. (2014, 2015), a shoulder visible in the N-XANES spectra of the Pluto/TNO tholins around 398–399 eV is consistent with the presence of imines, i.e., comparable to band N1 in our N-XANES spectra.

3.3. C/N ratios and nitrogen content

298

299 The elemental C/N abundance ratios derived from fitting the full-range XANES spectra (Fig. 4)
300 with atomic mass absorption coefficients (Henke et al., 1993; Section 2.2) for the four tholins
301 studied here are summarized in Table 2. The error bars on these ratios are due to the method used
302 to fit the XANES spectra to the atomic mass absorption coefficients (Cody et al., 2008; Nuevo et
303 al., 2011). C/N ratios were found to be low, in the 0.9–2.4 **range. These values** are consistent with
304 the C/N ratios **obtained using combustion and pyrolysis techniques** for other tholins produced
305 in experimental set-ups which use energy sources that can dissociate N_2 (i.e., cold plasma or
306 extreme UV radiation **sources) (Cable** et al., 2012). Note that an increase (respectively, decrease)
307 in the C/N ratio can be due to an increase (respectively, decrease) in the relative abundance of C
308 and/or a decrease (respectively, increase) in the relative abundance of N.

309 Our tholins produced **from gas** mixtures without acetylene display lower C/N ratios (0.9–
310 1.3) than those produced from mixtures with acetylene (2.2–2.4). This increase by a factor of 2 in
311 the C/N ratios of the tholin samples produced from the gas mixtures **with C_2H_2 is** correlated with
312 an increase in the abundance of aromatic carbon, imines, and nitriles observed in these samples
313 (Fig. 2, Section 3.1). These observations indicate that the addition of acetylene by as small a mixing
314 ratio as 0.5% in the initial gas mixture results in a significant increase in the formation of chemical
315 groups that consist of double and triple covalent bonds (C=C, C=N, and C≡N). In addition, the
316 nitrile band (band N2 in Fig. 3 and Table 1) of the tholin samples produced from mixtures that
317 contained acetylene tends to be shifted to higher energies, implying a larger proportion of nitrile
318 groups attached to aromatic structures, as opposed to aliphatic structures (band N2*) (Section **3.2).**

319 **A** plausible explanation for these observations resides in the design of the COSmIC/THS
320 experimental set-up, which only allows for the first steps of the chemistry to occur, due to the short

residence time (~3.5 μs) of the gas in the plasma discharge. This truncated chemistry was demonstrated by a mass spectrometry study of the plasma-generated gas-phase products (Sciamma-O'Brien et al., 2014), and subsequently confirmed by a modeling study of the gas phase (Raymond et al., 2018). These studies indicated that, in the COSmIC/THS experiment, plasmas generated in gas mixtures containing heavier molecular precursors result in the production of heavier molecular products. The presence of heavier precursors in the initial gas mixtures allows to go further into the chemical pathways associated with that precursor, leading to the formation of larger molecules within the short residence time of the gas in the plasma cavity. However, the use of heavier precursors can also lead to a chemistry favoring specific chemical pathways that involve these initial precursors and/or dominant products formed from these precursors.

In addition, in an IR spectroscopy study of the solid-phase products formed in the COSmIC/THS set-up (Sciamma-O'Brien et al., 2017), it was observed that both the nitrogen chemistry and the incorporation of N atoms into the solid phase vary depending on the composition of the initial gas mixture. In particular, when acetylene was present in the mixture, the chemistry appeared to favor the formation of aromatic hydrocarbons, in which fewer N atoms were incorporated into the tholins. The IR bands associated with N-bearing functional groups showed that N atoms were added to the periphery of the molecules rather than deeper inside the molecular structure, which is consistent with the findings of the present study. A possible explanation for the higher C/N ratios reported here for tholins produced from mixtures containing acetylene as well as from the IR spectroscopy results reported in Sciamma-O'Brien et al. (2017) is that the high reactivity of C_2H radicals produced from the dissociation of C_2H_2 (Herbst and Woon, 1997; Agúndez and Wakelam, 2013) triggers a chemistry in which the formation of hydrocarbons is favored over that of N-bearing molecules **during** the short 3.5-μs residence time of the gas in the

plasma cavity, which results in more aromatic hydrocarbons being formed and less nitrogen being incorporated in a bottom-up-type chemistry starting with smaller molecules.

When comparing the C/N ratios of the tholin samples produced from N_2:CH_4 and N_2:CH_4:C_2H_2 gas mixtures with different concentrations of CH_4, we also observe that an increase in the concentration of CH_4 (from 5% to 10%) results in a slight decrease in the C/N ratio for both the samples produced from N_2:CH_4 mixtures (from 1.3 to 0.9) and those produced from N_2:CH_4:C_2H_2 mixtures (from 2.4 to 2.2). Although this observation suggests that more N atoms may be incorporated into the tholins when the initial gas mixture contains more CH_4, in particular because this change in C/N ratio is observed for both N_2:CH_4 and N_2:CH_4:C_2H_2 mixtures, note that the uncertainties associated with the C/N ratio values (Table 2) are large enough for the C/N ratios to be considered as constant for a given gas composition (N_2:CH_4 or N_2:CH_4:C_2H_2) when the CH_4 concentration increases.

Our XANES results **are also consistent** with a previous IR study of our COSmIC/THS tholins (Sciamma-O'Brien et al., 2017), **in which** we observe**d** lower C/N ratios and smaller amounts of nitriles in tholins produced from the mixtures that did not contain C_2H_2. **The lower level of incorporation of nitrogen in the tholins formed from N_2:CH_4:C_2H_2 mixtures is also consistent with the findings of a recent study of the surface energy of tholins produced in the COSmIC set-up from N_2:CH_4 (95:5) and N_2:CH_4:C_2H_2 (94.5:5:0.5) gas mixtures (Li et al., 2021).** The effects of varying the concentration of CH_4 and/or adding acetylene as a precursor in the initial gas mixtures therefore reveal significant differences in how nitrogen is incorporated into the solid phase of our tholin samples.

3.4. Comparison with C/N ratios from the literature

From a general standpoint, it is difficult to conduct a rigorous comparison of the C/N ratios determined for the tholins of our study with other Titan tholins produced in previous, independent studies reported in the literature (e.g., McDonald et al., 1994; Coll et al., 1995, 1997, 1999, 2001; McKay, 1996; Sarker et al., 2003; Tran et al., 2003, 2008; Imanaka et al., 2004; Curtis et al., 2005; Ferris et al., 2005; Somogyi et al., 2005; Bernard et al., 2006; Szopa et al., 2006; Neish et al., 2008; Quirico et al., 2008; Sekine et al., 2008; Carrasco et al., 2009, 2016; Imanaka and Smith, 2010; Sciamma-O'Brien et al., 2010; Cable et al., 2012), as these tholins were produced using a wide range of experimental set-ups with many varying parameters (gas mixture composition, energy source, pressure, temperature, etc.) that could all have an impact on the final measured C/N ratios.

To the best of our knowledge, before the study presented here with the COSmIC experimental set-up, only two other experimental set-ups were used to conduct systematic C/N ratio studies of tholins produced with different concentrations of methane. McDonald et al. (1994) used a continuous flow plasma experiment at room temperature with a pressure of 1.5 mbar to produce tholins from N_2:CH_4 gas mixtures with 0.1% and 10% of CH_4 and did observe a decrease in the C/N ratio when increasing the CH_4 mixing ratio (C/N ratios of 1.49 and 0.75 for CH_4 concentrations of 0.1% and 10%, respectively), which is in agreement with the trend we observe in the COSmIC study presented here (C/N ratios of 0.9 and 1.3 for CH_4 concentrations of 5% and 10%, respectively). The opposite trend was reported for tholins produced in another experimental set-up (PAMPRE) at room temperature and 1–2 mbar pressure in a continuous flow plasma experiment (Quirico et al., 2008; Sciamma-O'Brien et al., 2010; Carrasco et al., 2016), where a higher C/N ratio was observed for tholins

produced with higher concentration of CH_4, with C/N ratios of 1.67 and 2.5 for CH_4 concentrations of 5% and 10%, respectively (Carrasco et al. 2016). These opposite trends in published data show the complexity of comparing the results obtained from different experiments.

For instance, if we look at the only other experimental set-up (PAMPRE) that was used to conduct systematic studies in which tholins were produced from concentrations of CH_4 of 5% and 10% and their C/N ratios were determined (Sciamma-O'Brien et al., 2010; Carrasco et al., 2016), an increase by a factor of 1.5 in the C/N ratio of the PAMPRE tholins was observed when increasing the concentration of CH_4 in the initial N_2:CH_4 gas mixture from 5% to 10%. This trend is the opposite of what we observe in the COSmIC tholins, where the C/N ratio decreases by a factor of 1.4 when the CH_4 concentration increases from 5% to 10% (Table 2, Section 3.3). In the PAMPRE experiment, however, a continuous plasma is used, and the set-up is designed so that the aerosols remain in levitation and grow in the plasma discharge for a long time (~100 s; Alcouffe et al., 2010). In contrast, in the COSmIC experiment, a pulsed plasma is used in the stream of an accelerated gas expansion, and the residence time of the gas in the plasma cavity is ~3.5 µs, which means that the residence time of the aerosols, which are carried by the accelerated pulsed gas expansion, is shorter than 3.5 µs (Sciamma-O'Brien et al., 2014). The very short residence time in COSmIC results in truncated chemistry and aerosol growth (Sciamma-O'Brien et al., 2014, 2017; Raymond et al. 2018), while the longer residence time in PAMPRE allows the chemistry to progress much farther. This difference could change the way nitrogen is incorporated into the solid phase and explain the opposite trends observed in the PAMPRE and COSmIC experiments.

Another difference between the PAMPRE and COSmIC experimental set-ups that could explain the opposite trends observed for the C/N ratios is the operating gas temperature in the reaction chamber (room temperature for PAMPRE vs. 150 K for COSmIC), which could result in different chemical pathways, changing the nitrogen incorporation into the solid phase. The significant effect of the operating gas temperature on the tholin C/N ratios has been demonstrated by Coll et al. (1999). In their experiments, Coll et al. produced tholins via plasma chemistry at room temperature and 100–150 K from N_2:CH_4 (98:2) gas mixtures at low pressure (1.5 mbar). The C/N ratios determined for the resulting tholins were 1.73 at room temperature and 2.82–2.83 at 100–150 K. This study thus highlights an important effect of the gas temperature on the chemistry and in particular the nitrogen incorporation, and may explain why the evolution of the C/N ratio as a function of the concentration of CH_4 in the initial mixture in our experiments is different from what is observed in the PAMPRE experiments.

Other factors like the gas pressure and the energy flux inducing the chemistry most likely also contribute to the differences observed in the chemistry and the nitrogen incorporation into the solid phase between the PAMPRE and COSmIC experimental set-ups. This demonstrate how difficult comparative analyses can be between different experimental set-ups. Only systematic and purposeful comparative studies where specific parameters are varied to observe their effects on the properties of the tholins (optical constants, physical and bulk properties, composition) will shed some light on the differences observed between different experimental set-ups. All three experimental set-ups that have conducted C/N ratio studies of tholins produced in different gas mixtures have however demonstrated that the

initial composition has an effect on the way nitrogen is incorporated into the solid phase, which is a piece of the puzzle to unveil the complexity of Titan's chemistry.

3.5. *Oxygen-bearing compounds and C/O ratios*

Although oxygen was not present in any of the initial starting gas mixtures, its contribution to the full-range XANES spectra is non negligible. Indeed, Fig. 4 shows that the intensity of the O edge is 5–8 and 2–4 times smaller than the intensities for the C and N edges, respectively. This means that a measurable amount of oxygen was incorporated into the tholins during the few minutes they were transferred onto the sample holders to be placed into the STXM device for XANES analysis. Oxidation of the tholin samples is supported by the presence of multiple oxygen-bearing functional groups in the C-XANES and N-XANES spectra of all tholins, in particular amides and alcohols (Table 1), as well as other types of carbonyls (Tables S1 and S2). The corresponding normalized O-XANES spectra of the four tholins produced in this study are shown in Fig. S1, while the complete list of the band assignments is given in Table S3, both in the Supplementary Material.

The presence of O-bearing groups in all our tholin samples may be explained by the structure of the tholin samples produced in these experiments. Because materials analyzed with the STXM instrument need to be thin enough for the X-rays to penetrate through the full thickness of the samples, the tholins studied here were produced from experiments that lasted 1–2 hours, resulting in substrates covered with scattered individual grains, 100–500 nm in diameter (depending on the initial mixture), separated from each other on the substrate. In contrast, during longer experiments, in which the tholins are typically recovered after 10–40 hours of sample production, the grains jet-deposited on the substrate stack on top of each other, forming a more

458 homogenous layer of material (Sciamma-O'Brien et al., 2017). Consequently, oxidation will affect
459 a larger fraction of the samples produced from shorter experiments, as the ratio between the surface
460 exposed to oxidation and the volume of material is much higher for samples consisting of
461 individual grains (i.e., shorter experiments) than for samples consisting of a homogenous deposit
462 (i.e., longer experiments). **In Carrasco et al. (2016), the layer of oxidation of a Titan tholin**
463 **sample produced from an oxygen-free N_2:CH_4 (90:10) initial mixture was measured to be**
464 **about 20 nm thick. Considering spherical grains with a diameter of 500 nm for our tholin**
465 **samples produced from gas mixtures containing C_2H_2 (Sciamma-O'Brien et al., 2017), a 20-**
466 **nm-thick oxidation layer would correspond to an oxidation level of about 22% of the total**
467 **volume. However, the tholin sample produced by Carrasco et al. (2016) was not kept under**
468 **inert atmosphere and was therefore exposed to air for a long period of time before**
469 **characterization. Since our tholin samples were kept under an argon atmosphere and**
470 **exposed to air for only a few minutes before being analyzed, the thickness of the oxidation**
471 **layer is expected to be smaller than 20 nm. Nonetheless, because the tholin samples produced**
472 **in our XANES study have a large surface-to-volume ratio, their** XANES **spectra are more**
473 susceptible to higher relative levels of oxidation, as confirmed by the high abundances of O-
474 bearing groups (Fig. S1, Table S3, Supplementary Material).

475 Kuga et al. (2014) also reported the presence of O-bearing functional groups in the C- and
476 N-XANES spectra of their Titan tholin sample produced from an oxygen-free N_2:CH_4 (95:5) initial
477 mixture. They observed bands associated with amides, alcohols, and ethers, which are also present
478 in all our tholin samples (Tables 1, S1, and S2). Previous tholin studies showed that unsaturated
479 chemical groups in the molecular structure of tholins produced by cold plasmas are dominated by

480 nitrogen-bearing moieties (i.e., imines, nitriles), which may explain why tholins are easily prone
481 to hydrolysis and therefore oxidation (Cable et al., 2012).

482 Finally, the elemental C/O abundance ratios (and their associated error bars) derived for
483 the four tholins studied here (see Sections 2.2 and 3.3.) are summarized in Table S4
484 (Supplementary Material). These ratios were determined to range from 1.9 to 3.3, with higher C/O
485 ratios for tholins produced from initial mixtures containing acetylene. A previous scanning
486 electron microscopy (SEM) study of COSmIC/THS tholin samples (Sciamma-O'Brien et al., 2017)
487 demonstrated that tholins produced from N_2:CH_4:C_2H_2 gas mixtures consist of grains with much
488 larger diameter than tholins produced from simpler N_2:CH_4 mixtures (500 nm vs. 100 nm). This
489 implies that the surface-to-volume ratio of the tholin samples produced from C_2H_2-containing
490 mixtures is much smaller than for tholins produced in mixtures without C_2H_2, which results in less
491 oxidation of the samples when exposed to air. The observation of lower C/O ratios for the tholins
492 produced in C_2H_2-containing mixtures are therefore consistent with the hypothesis that oxidation
493 most probably occurred when the tholins were exposed to air during their transfer to the sample
494 holder to be analyzed with the STXM instrument rather than during the experiments inside the
495 COSmIC/THS chamber.

496

497 ***3.6.*** *Applications to Titan's atmosphere*

498

499 The XANES study at the C and N edges of the tholin samples produced in our COSmIC/THS
500 experimental set-up from four different initial gas mixtures, namely, N_2:CH_4 (90:10 and 95:5) and
501 N_2:CH_4:C_2H_2 (89.5:10:0.5 and 94.5:5:0.5), showed that the relative abundances between the C-
502 and N-bearing products that are formed vary with both the presence or absence of C_2H_2 and

503 **possibly** the relative proportion of CH_4 in the initial gas mixtures. XANES spectra of these tholins
504 also showed that mixtures containing C_2H_2 favored the formation of aromatic compounds and
505 larger relative amounts of imines and nitriles compared with when C_2H_2 is not present.
506 These important results can be used to infer some connections with what can be expected
507 for the production mechanisms of the aerosols that are responsible for the haze layers in Titan's
508 atmosphere. Indeed, the variations observed for the composition and C/N ratios of our four tholin
509 samples can be interpreted as potential indicators of variations in the composition of Titan's haze,
510 as predicted by photochemical models (Wilson and Atreya, 2003; Lavvas et al., 2008a, 2008b).
511 Our experimental results **confirm that** the nitrogen content of Titan's aerosols **is** expected **to vary**
512 over seasonal and astronomical timescales (Lunine and Atreya, 2008; Roe, 2012).
513 The nitrogen content of Titan's aerosols is also expected to vary as a function of the altitude
514 and latitude at which the aerosols are formed, particularly during seasonal changes that affect the
515 atmospheric circulation and result in a molecular enrichment at the poles**. For example, molecules**
516 **such as C_2H_2, C_2H_4, C_2H_6, C_6H_6, HC_3N, and HCN were observed in higher concentrations at**
517 **the south pole after the northern spring equinox, where they are expected to have an impact**
518 **on the composition of the aerosols formed at these latitudes** (e.g., Teanby et al., 2012; Vinatier
519 et al., 2015; Coustenis et al., 2016; Mathé et al., 2020). Our experimental results demonstrate that
520 a change in the atmospheric composition due to these seasonal and local enhancements would
521 influence the chemistry and the resulting aerosol production mechanisms. The low C/N ratios
522 measured for all our tholin samples are also consistent with the hypothesis that Titan's aerosols
523 act as a sink for N atoms in the atmosphere, as supported by the data collected by *Huygens*' Aerosol
524 Collector Pyrolyser (Israël et al., 2005).
525

4. Conclusions

We produced Titan tholins in the COSmIC/THS experimental set-up using a plasma discharge in the stream of a jet-cooled expansion for four different initial gas mixtures: N_2:CH_4 (90:10), N_2:CH_4 (95:5), N_2:CH_4:C_2H_2 (89.5:10:0.5), and N_2:CH_4:C_2H_2 (94.5:5:0.5). The tholin samples were collected under inert atmosphere after 1–2 hours of deposition and were analyzed with XANES spectroscopy at the C, N, and O edges. The absorption bands identified in the XANES spectra of these tholin samples indicate the presence of various chemical structures and groups, including aromatic carbon, imines, and nitriles. The relative abundances between these bands vary with (i) the presence or absence of C_2H_2, and (ii) **possibly** the concentration of CH_4 in the initial mixtures. COSmIC/THS experiments conducted with initial mixtures in which C_2H_2 was added resulted in the formation of tholins that contain more aromatic compounds and larger relative amounts of imines and nitriles compared with tholins produced from mixtures that did not contain C_2H_2. XANES spectra of all tholins also show the presence of O-bearing species that resulted from the oxidation of the tholins when exposed to **air. Furthermore**, XANES analysis allowed for the determination of the elemental C, N, and O composition of our four tholin samples, and the subsequent estimate of their C/N and C/O ratios. C/N ratios were all found to be low (< 2.5), in agreement with previous, independent studies of tholins produced with energy sources that can dissociate N_2. **C/N ratios were found to be slightly lower when the concentration of CH_4 in the gas mixture was higher. Finally**, the C/N ratios of tholins produced from gas mixtures that contained **C_2H_2 were** found to be twice as large as of those produced from mixtures that did not contain **C_2H_2, demonstrating the impact of the composition of the initial gas on the composition of the resulting solid-phase particles, in particular the nitrogen incorporation.**

549 The differences in chemical (aromatic vs. aliphatic compounds, nitriles, etc.) and elemental
550 (C/N ratios) compositions, observed for our COSmIC/THS tholins produced from gas mixtures
551 with different concentrations of CH_4 and in the absence/presence of C_2H_2, highlight differences in
552 how nitrogen is incorporated into the solid phase: when C_2H_2 is absent from the initial mixture,
553 nitrogen is incorporated deeper in the molecular structure and nitrile groups are preferably attached
554 to aliphatic structures, while when C_2H_2 is present, nitrogen is added to the periphery of aromatic
555 molecules, for example in the form of nitrile groups.

556 Our experimental results can also guide the analysis of observations of Titan's atmosphere
557 and the development of models. Indeed, the differences in chemical and elemental compositions
558 of our tholins illustrate how a change in composition at the location where aerosols are formed in
559 Titan's atmosphere may lead to variations in the nitrogen content and composition of Titan's
560 aerosols. This variability depends on several parameters which need to be taken into account in
561 models, such as the location (altitude, latitude), the season, and the astronomical timescales, as
562 they can affect the atmospheric circulation, the concentration of specific molecules in different
563 parts of the atmosphere, and therefore the chemistry and product formation.

564

565 **Acknowledgments**

566

567 M. Nuevo, S. A. Sandford, and C. K. Materese acknowledge the NASA Emerging Worlds Program
568 and NASA Astrobiology Institute for funding. E. Sciamma-O'Brien and F. Salama acknowledge
569 the NASA SMD SERA Directed Work Package for funding. Finally, this research used resources
570 of beamline 5.3.2.2. at the Advanced Light Source, a U.S. DOE Office of Science User Facility
571 under contract no. DE-AC02-05CH11231.

572 **References**

573

574 Agúndez, M., Wakelam, V., 2013. Chemistry of dark clouds: Databases, networks, and models.
575 Chem. Rev., 113, 8710–8737. https://doi.org/10.1021/cr4001176

576 **Alcouffe, G., Cavarroc, M., Cernogora, G., Ouni, F., Jolly, A., Boufendi, L., Szopa, C., 2010.**
577 **Capacitively coupled plasma used to simulate Titan's atmospheric chemistry. Plasma**
578 **Sources Sci. Technol. 19, 015008 (11 pp). https://doi.org/10.1088/0963-0252/19/1/015008**

579 Apen, E., Hitchcock, A.P., Gland, J.L., 1993. Experimental studies of the core excitation of
580 imidazole, 4,5-dicyanoimidazole, and *s*-triazine. J. Phys. Chem. 97, 6859–6866.
581 https://doi.org/10.1021/j100128a019

582 Bajt, S., Chapman, H.N., Flynn, G.J., Keller, L.P., 1996. Carbon characterization in interplanetary
583 dust particles with a scanning transmission X-ray microscope. Lunar Planet. Sci. 27, 57–58.

584 Barnes, J.W., Turtle, E.P., Trainer, M.G., Lorenz, R.D., MacKenzie, S.M., Brinckerhoff, W.B.,
585 Cable, M.L., Ernst, C.M., Freissinet, C., Hand, K.P., Hayes, A.G., Hörst, S.M., Johnson, J.R.,
586 Karkoschka, E., Lawrence, D.J., Le Gall, A., Lora, J.M., McKay, C.P., Miller, R.S., Murchie,
587 S.L., Neish, C.D., Newman, C.E., Núñez, J., Panning, M.P., Parsons, A.M., Peplowski, P.N.,
588 Quick, L.C., Radebaugh, J., Rafkin, S.C.R., Shiraishi, H., Soderblom, J.M., Sotzen, K.S.,
589 Stickle, A.M., Stofan, E.R., Szopa, C., Tokano, T., Wagner, T., Wilson, C., Yingst, R.A.,
590 Zacny, K., Stähler, S.C., 2021. Science goals and objectives for the Dragonfly Titan rotorcraft
591 relocatable lander. Planet. Sci. J. 2, 130 (18 pp). https://doi.org/10.3847/PSJ/abfdcf

592 Bernard, J.-M., Quirico, E., Brissaud, O., Montagnac, G., Reynard, B., McMillan, P., Coll, P.,
593 Nguyen, M.-J., Raulin, F., Schmitt, B., 2006. Reflectance spectra and chemical structure of

Titan's tholins: Application to the analysis of Cassini–Huygens observations. Icarus 185, 301–307. https://doi.org/10.1016/j.icarus.2006.06.004

Biennier, L., Benidar, A., Salama, F., 2006. Flow dynamics of a pulsed planar expansion. Chem. Phys. 326, 445–457. https://doi.org/10.1016/j.chemphys.2006.03.016

Brassé, C., Muñoz, O., Coll, P., Raulin, F., 2015. Optical constants of Titan aerosols and their tholins analogs: Experimental results and modeling/observational data. Planet. Space Sci. 109–110, 159–174. https://doi.org/10.1016/j.pss.2015.02.012

Broks, B.H.P, Brok, W.J.M., Remy, J., van der Mullen, J.J.A.M., Benidar, A., Biennier, L., Salama, F., 2005. Numerical investigation of the discharge characteristics of the pulsed discharge nozzle. Phys. Rev. E 71, 036409 (8 pp). https://doi.org/10.1103/PhysRevE.71.036409

Cable, M.L., Hörst, S.M., Hodyss, R., Beauchamp, P.M., Smith, M.A., Willis, P.A., 2012. Titan tholins: Simulating Titan organic chemistry in the Cassini-Huygens era. Chem. Rev. 112, 1882–1909. https://doi.org/10.1021/cr200221x

Carrasco, N., Jomard, F., Vigneron, J., Etcheberry, A., Cernogora, G., 2016. Laboratory analogues simulating Titan's atmospheric aerosols: Compared chemical compositions of grains and thin films. Planet. Space Sci. 128, 52–57. https://doi.org/10.1016/j.pss.2016.05.006

Carrasco, N., Schmitz-Afonso, I., Bonnet, J-Y., Quirico, E., Thissen, R., Dutuit, O., Bagag, A., Laprévote, O., Buch, A., Giulani, A., Adandé, G., Ouni, F., Hadamcik, E., Szopa, C., Cernogora, G., 2009. Chemical characterization of Titan's tholins: Solubility, morphology and molecular structure revisited. J. Phys. Chem. A, 113, 11195–11203. https://doi.org/10.1021/jp904735q

Cherchneff, I., Barker, J.R., Tielens, A.G.G.M., 1992. Polycyclic aromatic hydrocarbon formation in carbon-rich stellar envelopes. Astrophys. J. 401, 269–287. https://doi.org/10.1086/172059

Cody, G.D., Ade, H., Alexander, C.M.O'D., Araki, T., Butterworth, A., Fleckenstein, H., Flynn, G., Gilles, M.K., Jacobsen, C., Kilcoyne, A.L.D., Messenger, K., Sandford, S.A., Tyliszczak, T., Westphal, A.J., Wirick, S., Yabuta, H., 2008. Quantitative organic and light-element analysis of comet 81P/Wild 2 particles using C-, N-, and O-μ-XANES. Meteorit. Planet. Sci. 43, 353–365. https://doi.org/10.1111/j.1945-5100.2008.tb00627.x

Cody, G.D., Gupta, N.S., Briggs, D.E.G., Kilcoyne, A.L.D., Summons, R.E., Kenig, F., Plotnick, R.E., Scott, A.C., 2011. Molecular signature of chitin-protein complex in Paleozoic arthropods. Geology 39, 255–258. https://doi.org/10.1130/G31648.1

Coll, P., Coscia, D., Gazeau, M.-C., Raulin, F., 1997. New planetary atmosphere simulations: Application to the organic aerosols of Titan. Adv. Space Res. 19, 1113–1119. https://doi.org/10.1016/S0273-1177(97)00360-8

Coll, P., Coscia, D., Gazeau, M.C., de Vanssay, E., Guillemin, J.C., Raulin, F., 1995. Organic chemistry in Titan's atmosphere: New data from laboratory simulations at low temperature. Adv. Space Res. 16, 93–103. https://doi.org/10.1016/0273-1177(95)00197-M

Coll, P., Coscia, D., Smith, N., Gazeau, M.-C., Ramírez, S.I., Cernogora, G., Israël, G., Raulin, F., 1999. Experimental laboratory simulation of Titan's atmosphere: aerosols and gas phase. Planet. Space Sci. 47, 1331–1340. https://doi.org/10.1016/S0032-0633(99)00054-9

Coll, P., Navarro-González, R., Szopa, C., Poch, O., Ramírez, S.I., Coscia, D., Raulin, F., Cabane, M., Buch, A., Israël, G., 2013. Can laboratory tholins mimic the chemistry producing Titan's aerosols? A review in light of ACP experimental results. Planet. Space Sci. 77, 91–103. https://doi.org/10.1016/j.pss.2012.07.006

639 Coll, P., Ramirez, S.I., Navarro-Gonzalez, R., Raulin, F., 2001. Chemical and optical behaviour
640 of tholins, laboratory analogues of Titan aerosols. Adv. Space Res. 27, 289–297.
641 https://doi.org/10.1016/S0273-1177(01)00060-6
642 Contreras, C.S., Salama, F., 2013. Laboratory investigations of polycyclic aromatic hydrocarbon
643 formation and destruction in the circumstellar outflows of carbon stars. Astrophys. J. Suppl.
644 Ser. 208, 6 (17 pp). https://doi.org/10.1088/0067-0049/208/1/6
645 Coustenis, A., Jennings, D.E., Achterberg, R.K., Bampasidis, G., Lavvas, P., Nixon, C.A., Teanby,
646 N.A., Anderson, C.M., Cottini, V., Flasar, F.M., 2016. Titan's temporal evolution in
647 stratospheric trace gases near the poles. Icarus 270, 409–420. https://doi.org/10.1016/
648 j.icarus.2015.08.027
649 Curtis, D.B., Glandorf, D.L., Toon, O.B., Tolbert, M.A., McKay, C.P., Khare, B.N., 2005.
650 Laboratory studies of butane nucleation on organic haze particles: Application to Titan's
651 clouds. J. Phys. Chem. A 109, 1382–1390. https://doi.org/10.1021/jp045596h
652 De Gregorio, B.T., Stroud, R.M., Nittler, L.R., Alexander, C.M.O'D., Bassim, N.D., Cody, G.D.,
653 Kilcoyne, A.L.D., Sandford, S.A., Milam, S.N., Nuevo, M., Zega, T.J., 2013. Isotopic and
654 chemical variation of organic nanoglobules in primitive meteorites. Meteorit. Planet. Sci. 48,
655 904–928. https://doi.org/10.1111/maps.12109
656 Dhez, O., Ade, H., Urquhart, S.G., 2003. Calibrated NEXAFS spectra of some common polymers.
657 J. Elec. Spec. Rel. Phenom. 128, 85–96. https://doi.org/10.1016/S0368-2048(02)00237-2
658 Díaz, J., Anders, S., Zhou, X., Moler, E.J., Kellar, S.A., Hussain, Z., 2001. Analysis of the π* and
659 σ* bands of the x-ray absorption spectrum of amorphous carbon. Phys. Rev. B 64, 125204 (9
660 pp). https://doi.org/10.1103/PhysRevB.64.125204

Ferris, J., Tran, B., Joseph, J., Vuitton, V., Briggs, R., Force, M., 2005. The role of photochemistry in Titan's atmospheric chemistry. Adv. Space Res. 36, 251–257. https://doi.org/10.1016/j.asr.2005.03.056

Frenklach, M., Feigelson, E.D., 1989. Formation of polycyclic aromatic hydrocarbons in circumstellar envelopes. Astrophys. J. 341, 372–384. https://doi.org/10.1086/167501

Fulchignoni, M., Ferri, F., Angrilli, F., Ball, A.J., Bar-Nun, A., Barucci, M.A., Bettanini, C., Bianchini, G., Borucki, W., Colombatti, G., Coradini, M., Coustenis, A., Debei, S., Falkner, P., Fanti, G., Flamini, E., Gaborit, V., Grard, R., Hamelin, M., Harri, A.M., Hathi, B., Jernej, I., Leese, M.R., Lehto, A., Lion Stoppato, P.F., López-Moreno, J.J., Mäkinen, T., McDonnell, J.A.M., McKay, C.P., Molina-Cuberos, G., Neubauer, F.M., Pirronello, V., Rodrigo, R., Saggin, B., Schwingenschuh, K., Seiff, A., Simões, F., Svedhem, H., Tokano, T., Towner, M.C., Trautner, R., Withers, P., Zarnecki, J.C., 2005. In situ measurements of the physical characteristics of Titan's environment. Nature 438, 785–791. https://doi.org/10.1038/nature04314

Gordon, M.L., Cooper, G., Morin, C., Araki, T., Turci, C.C., Kaznatcheev, K., Hitchcock, A.P., 2003. Inner-shell excitation spectroscopy of the peptide bond: Comparison of the C 1*s*, N 1*s*, and O 1*s* spectra of glycine, glycyl–glycine, and glycyl–glycyl–glycine. J. Phys. Chem. A 107, 6144–6159. https://doi.org/10.1021/jp0344390

Hanel, R., Conrath, B., Flasar, F.M., Kunde, V.G., Maguire, W., Pearl, J., Pirraglia, J., Samuelson, R.E., Herath, L., Allison, M., Cruikshank, D.P., Gautier, D., Gierasch, P., Horn, L., Koppany, R., Ponnamperuma, C., 1981. Infrared observations of the Saturnian system from Voyager 1, Science 212, 192–200. https://doi.org/10.1126/science.212.4491.192

He, C., Hörst, S.M., Riemer, S., Sebree, J.A., Pauley, N., Vuitton, V., 2017. Carbon monoxide affecting planetary atmospheric chemistry. Astrophys. J. Lett. 841, L31 (7 pp). https://doi.org/10.3847/2041-8213/aa74cc

He, C., Smith, M.A., 2014. Identification of nitrogenous organic species in Titan aerosols analogs: Implication for prebiotic chemistry on Titan and early Earth. Icarus 238, 86–92. https://doi.org/10.1016/j.icarus.2014.05.012

Henke, B.L., Gullikson, E.M., Davis, J.C., 1993. X-ray interactions: Photoabsorption, scattering, transmission, and reflection at E = 50–30,000 eV, Z = 1–92. Atom. Data Nucl. Data Tab. 54, 181–342. https://doi.org/10.1006/adnd.1993.1013

Herbst, E., Woon, D.E., 1997. The rate of the reaction between C_2H and C_2H_2 at interstellar temperatures. Astrophys. J. 489, 109–112. https://doi.org/10.1086/304786

Hörst, S.M. (2017) Titan's atmosphere and climate. J. Geophys. Res. Planets 122, 432–482. https://doi.org/10.1002/2016JE005240

Imanaka, H., Khare, B.N., Elsila, J.E., Bakes, E.L.O., McKay, C.P., Cruikshank, D.P., Sugita, S., Matsui, T., Zare, R.N., 2004. Laboratory experiments of Titan tholin formed in cold plasma at various pressures: implications for nitrogen-containing polycyclic aromatic compounds in Titan haze. Icarus 168, 344–366. https://doi.org/10.1016/j.icarus.2003.12.014

Imanaka, H., Smith, M.A., 2010. Formation of nitrogenated organic aerosols in the Titan upper atmosphere. Proc. Natl. Acad. Sci. 107, 12423–12428. https://doi.org/10.1073/pnas.0913353107

Ishii, I., Hitchcock, A.P., 1988. The oscillator strengths for C1*s* and O1*s* excitation of some saturated and unsaturated organic alcohols, acids and esters. J. Elec. Spec. Rel. Phenom. 46, 55–84. https://doi.org/10.1016/0368-2048(88)80005-7

706 Israël, G., Szopa, C., Raulin, F., Cabane, M., Niemann, H.B., Atreya, S.K., Bauer, S.J., Brun, J.-
707 F., Chassefière, E., Coll, P., Condé, E., Coscia, D., Hauchecorne, A., Millian, P., Nguyen, M.-
708 J., Owen, T., Riedler, W., Samuelson, R.E., Siguier, J.-M., Steller, M., Sternberg, R., Vidal-
709 Madjar, C., 2005. Complex organic matter in Titan's atmospheric aerosols from *in situ*
710 pyrolysis and analysis. Nature 438, 796–799. https://doi.org/10.1038/nature04349
711 Jäger, C., Huisken, F., Mutschke, H., Llamas Jansa, I., Henning, T., 2009. Formation of polycyclic
712 aromatic hydrocarbons and carbonaceous solids in gas-phase condensation experiments.
713 Astrophys. J. 696, 706–712. https://doi.org/10.1088/0004-637X/696/1/706
714 Keller, L.P., Messenger, S., Flynn, G.J., Clemett, S., Wirick, S., Jacobsen, C., 2004. The nature of
715 molecular cloud material in interplanetary dust. Geochim. Cosmochim. Acta 68, 2577–2589.
716 https://doi.org/10.1016/j.gca.2003.10.044
717 Kikuma, J., Warwick, T., Shin, H.-J., Zhang, J., Tonner, B.P., 1998. Chemical state analysis of
718 heat-treated polyacrylo-nitrile fiber using soft X-ray spectromicroscopy. J. Elec. Spec. Rel.
719 Phenom. 94, 271–278. https://doi.org/10.1016/S0368-2048(98)00196-0
720 Kilcoyne, A.L.D., Tyliszczak, T., Steele, W.F., Fakra, S., Hitchcock, P., Franck, K., Anderson, E.,
721 Harteneck, B., Rightor, E.G., Mitchell, G.E., Hitchcock, A.P., Yang, L., Warwick, T., Ade, H.,
722 2003. Interferometer-controlled scanning transmission X-ray microscopes at the Advanced
723 Light Source. J. Synchr. Rad. 10, 125–136. https://doi.org/10.1107/S0909049502017739
724 Kuga, M., Carrasco, N., Marty, B., Marrocchi, Y., Bernard, S., Rigaudier, T., Fleury, B., Tissandier,
725 L., 2014. Nitrogen isotopic fractionation during abiotic synthesis of organic solid particles.
726 Earth Planet. Sci. Lett. 393, 2–13. https://doi.org/10.1016/j.epsl.2014.02.037

727 Lavvas, P.P., Coustenis, A., Vardavas, I.M., 2008a. Coupling photochemistry with haze formation
728 in Titan's atmosphere, Part I: Model description. Planet. Space Sci. 56, 27–66. https://doi.org/
729 10.1016/j.pss.2007.05.026
730 Lavvas, P.P., Coustenis, A., Vardavas, I.M., 2008b. Coupling photochemistry with haze formation
731 in Titan's atmosphere, Part II: Results and validation with Cassini/Huygens data. Planet. Space
732 Sci. 56, 67–99. https://doi.org/10.1016/j.pss.2007.05.027
733 Lebreton, J.-P., Witasse, O., Sollazzo, C., Blancquaert, T., Couzin, P., Schipper, A.-M., Jones, J.B.,
734 Matson, D.L., Gurvits, L.I., Atkinson, D.H., Kazeminejad, B., Pérez-Ayúcar, M., 2005. An
735 overview of the descent and landing of the Huygens probe on Titan. Nature 438, 758–764.
736 https://doi.org/10.1038/nature04347
737 Lehmann, J., Liang, B., Solomon, D., Lerotic, M., Luizão, F., Kinyangi, J., Schäfer, T., Wirick S.,
738 Jacobsen, C., 2005. Near-edge X-ray absorption fine structure (NEXAFS) spectroscopy for
739 mapping nanoscale distribution of organic carbon forms in soil: Application to black carbon
740 particles. Global Biogeochem. Cycles 19, 1013–1025. https://doi.org/10.1029/2004GB002435
741 Leinweber, P., Kruse, J., Walley, F.L., Gillespie, A., Eckhardt, K.-U., Blyth, R., Regier, T., 2007.
742 Nitrogen K-edge XANES – An overview of reference compounds used to identify 'unknown'
743 organic nitrogen in environmental samples. J. Synchr. Rad. 14, 500–511. https://doi.org/
744 10.1107/S0909049507042513
745 **Li, J., Yu, X., Sciamma-O'Brien, E., He, C., Sebree, J.A., Salama, F., Hörst, S.M., Zhang, X.,**
746 **2021. A cross-laboratory comparison study of Titan haze analogs: Surface energy. Planet.**
747 **Sci. J. (accepted).**

748 Lindal, G.F., Wood, G.E., Hotz, H.B., Sweetnam, D.N., Eshleman, V.R., Tyler, G.L., 1983. The
749 atmosphere of Titan: An analysis of the Voyager 1 radio occultation measurements. Icarus 53,
750 348–363. https://doi.org/10.1016/0019-1035(83)90155-0
751 Lunine, J.I., Atreya, S.K., 2008. The methane cycle on Titan. Nat. Geosci. 1, 159–164.
752 https://doi.org/10.1038/ngeo125
753 Maillard, J., Schmitz-Afonso, I., Gautier, T., Afonso, C., Carrasco, N., 2021. Suggested plausible
754 structures for Titan's haze analogs using tandem mass spectrometry. Icarus 358, 114181 (8 pp).
755 https://doi.org/10.1016/j.icarus.2020.114181
756 Materese, C.K., Cruikshank, D.P., Sandford, S.A., Imanaka, H., Nuevo, M., 2015. Ice chemistry
757 on outer Solar System bodies: Electron radiolysis of N_2-, CH_4-, and CO-containing ices.
758 Astrophys. J. 812, 150 (9 pp). https://doi.org/10.1088/0004-637X/812/2/150
759 Materese, C.K., Cruikshank, D.P., Sandford, S.A., Imanaka, H., Nuevo, M., White, D.W., 2014.
760 Ice chemistry on outer Solar System bodies: Carboxylic acids, nitriles, and urea detected in
761 refractory residues produced from the UV photolysis of N_2:CH_4:CO-containing ices.
762 Astrophys. J. 788, 111 (11 pp). https://doi.org/10.1088/0004-637X/788/2/111
763 Mathé, C., Vinatier, S., Bézard, B., Lebonnois, S., Gorius, N., Jennings, D.E., Mamoutkine, A.,
764 Guandique, E., Vatant d'Ollone, J., 2020. Seasonal changes in the middle atmosphere of Titan
765 from Cassini/CIRS observations: Temperature and trace species abundance profiles from 2004
766 to 2017. Icarus 344, 113547 (27 pp). https://doi.org/10.1016/j.icarus.2019.113547
767 Matrajt, G., Ito, M., Wirick, S., Messenger, S., Brownlee, D.E., Joswiak, D., Flynn, G., Sandford,
768 S., Snead, C., Westphal, A., 2018. Carbon investigation of two Stardust particles: A TEM,
769 NanoSIMS, and XANES study. Meteorit. Planet. Sci. 43, 315–334. https://doi.org/10.1111/
770 j.1945-5100.2008.tb00625.x

771 Matson, D.L., Spilker, L.J., Lebreton, J.-P., 2002. The Cassini/Huygens Mission to the Saturnian
772 System. Space Sci. Rev. 104, 1–58. https://doi.org/10.1023/A:1023609211620
773 Matson, D.L., Spilker, L.J., Lebreton, J.-P., 2003. The Cassini/Huygens Mission to the Saturnian
774 System. In: Russell, C.T., eds., Springer, Dordrecht. https://doi.org/10.1007/978-94-017-3251-
775 2_1
776 McDonald, G.D., Thompson, W.R., Heinrich, M., Khare, B.N., Carl Sagan, C., 1994. Chemical
777 investigation of Titan and Triton tholins. Icarus 108, 137–145. https://doi.org/10.1006/
778 icar.1994.1046
779 McKay, C.P., 1996. Elemental composition, solubility, and optical properties of Titan's organic
780 haze. Planet. Space Sci. 44, 741–747. https://doi.org/10.1016/0032-0633(96)00009-8
781 Mitchell, R.T., 2006. Cassini/Huygens at Saturn and Titan. Acta Astronautica 59, 335–343.
782 https://doi.org/10.1016/j.actaastro.2006.02.040
783 Neish, C.D., Somogyi, Á., Imanaka, H., Lunine, J.I., Smith, M.A., 2008. Rate measurements of
784 the hydrolysis of complex organic macromolecules in cold aqueous solutions: Implications for
785 prebiotic chemistry on the early Earth and Titan. Astrobiology 8, 273–287. https://doi.org/
786 10.1089/ast.2007.0193
787 Niemann, H.B., Atreya, S. K., Demick, J.E., Gautier, D., Haberman, J. A., Harpold, D.N.,
788 Kasprzak, W.T., Lunine, J.I., Owen, T.C., Raulin, F., 2010. Composition of Titan's lower
789 atmosphere and simple surface volatiles as measured by the Cassini-Huygens probe gas
790 chromatograph mass spectrometer experiment. J. Geophys. Res. 115, E12006 (22 pp).
791 https://doi.org/10.1029/2010JE003659

792 Nuevo, M., Milam, S.N., Sandford, S.A., De Gregorio, B.T., Cody, G.D., Kilcoyne, A.L.D., 2011.
793 XANES analysis of organic residues produced from the UV irradiation of astrophysical ice
794 analogs. Adv. Space Res. 48, 1126–1135. https://doi.org/10.1016/j.asr.2011.05.020
795 Owen, T., 2005. Huygens rediscovers Titan. Nature 438, 756–757. https://doi.org/10.1038/
796 438756a
797 Pels, J.R., Kapteijn, F., Moulijn, J.A., Zhu, Q., Thomas, K.M., 1995. Evolution of nitrogen
798 functionalities in carbonaceous materials during pyrolysis. Carbon 33, 1641–1653.
799 https://doi.org/10.1016/0008-6223(95)00154-6
800 Quirico, E., Montagnac, G., Lees, V., McMillan, P.F., Szopa, C., Cernogora, G., Rouzaud, J.-N.,
801 Simon, P., Bernard, J.-M., Coll, P., Fray, N., Minard, R.D., Raulin, F., Reynard, B., Schmitt,
802 B., 2008. New experimental constraints on the composition and structure of tholins. Icarus 198,
803 218–231. https://doi.org/10.1016/j.icarus.2008.07.012
804 Raulin, F., Brassé, C., Poch, O., Coll, P., 2012. Prebiotic-like chemistry on Titan. Chem. Soc. Rev.
805 41, 5380–5393. https://doi.org/10.1039/C2CS35014A
806 Ray, S.C., Pao, C.W., Chiou, J.W., Tsai, H.M., Jan, J.C., Pong, W.F., McCann, R., Roy, S.S.,
807 Papakonstantinou, P., McLaughlin, J.A., 2005. Electronic properties of *a*-CN_x thin films: An
808 x-ray-absorption and photoemission spectroscopy study. J. Appl. Phys. 98, 033708 (4 pp).
809 https://doi.org/10.1063/1.1994933
810 Raymond, A.W., Sciamma-O'Brien, E., Salama, F., Mazur, E., 2018. A model of Titan-like
811 chemistry to connect experiments and *Cassini* observations. Astrophys. J. 853, 107 (17 pp).
812 https://doi.org/10.3847/1538-4357/aaa12c
813 Roe, H.G., 2012. Titan's methane weather. Annu. Rev. Earth Planet. Sci. 40, 355–382.
814 https://doi.org/10.1146/annurev-earth-040809-152548

Sagan, C., Khare, B.N., 1979. Tholins: Organic chemistry of interstellar grains and gas. Nature 277, 102–107. https://doi.org/10.1038/277102a0

Salama, F., Sciamma-O'Brien, E., Contreras, C.S., Bejaoui, S., 2018. Recent progress in laboratory astrophysics achieved with NASA Ames' COSmIC facility. Proc. IAU S332, 13, 364–369. https://doi.org/10.1017/S1743921317011619

Sandford, S.A., Aléon, J., Alexander, C.M.O'D., Araki, T., Bajt, S., Baratta, G.A., Borg, J., Bradley, J.P., Brownlee, D.E., Brucato, J.R., Burchell, M.J., Busemann, H., Butterworth, A., Clemett, S.J., Cody, G., Colangeli, L., Cooper, G., d'Hendecourt, L., Djouadi, Z., Dworkin, J.P., Ferrini, G., Fleckenstein, H., Flynn, G.J., Franchi, I.A., Fries, M., Gilles, M.K., Glavin, D.P., Gounelle, M., Grossemy, F., Jacobsen, C., Keller, L.P., Kilcoyne, A.L.D., Leitner, J., Matrajt, G., Meibom, A., Mennella, V., Mostefaoui, S., Nittler, L.R., Palumbo, M.E., Papanastassiou, D.A., Robert, F., Rotundi, A., Snead, C.J., Spencer, M.K., Stadermann, F.J., Steele, A., Stephan, T., Tsou, P., Tyliszczak, T., Westphal, A.J., Wirick, S., Wopenka, B., Yabuta, H., Zare, R.N., Zolensky, M.E., 2006. Organics captured from comet 81P/Wild 2 by the Stardust spacecraft. Science 314, 1720–1724. https://doi.org/10.1126/science.1135841

Sarker, N., Somogyi, A., Lunine, J.I., Smith, M.A., 2003. Titan aerosol analogues: Analysis of the nonvolatile tholins. Astrobiology 3, 719–726. https://doi.org/10.1089/153110703322736042

Sciamma-O'Brien, E., Carrasco, N., Szopa, C., Buch, A., Cernogora, G., 2010. Titan's atmosphere: An optimal gas mixture for aerosol production? Icarus 209, 704–714. https://doi.org/10.1016/j.icarus.2010.04.009

Sciamma-O'Brien, E., Ricketts, C.L., Salama, F., 2014. The Titan Haze Simulation experiment on COSmIC: Probing Titan's atmospheric chemistry at low temperature. Icarus 243, 325–336. https://doi.org/10.1016/j.icarus.2014.08.004

838 Sciamma-O'Brien, E., Upton, K.T., Salama, F., 2017. The Titan Haze Simulation (THS)
839 experiment on COSmIC. Part II. Ex-situ analysis of aerosols produced at low temperature.
840 Icarus 289, 214–226. https://doi.org/10.1016/j.icarus.2017.02.004
841 Schulz, F., Maillard, J., Kaiser, K., Schmitz-Afonso, I., Gautier, T., Afonso, C., Carrasco, N.,
842 Gross, L., 2021. Imaging Titan's organic haze at atomic scale. Astrophys. J. Lett. 908, L13
843 (11pp). https://doi.org/10.3847/2041-8213/abd93e
844 Sebree, J.A., Roach, M.C., Shipley, E.R., He, C., Hörst, S.M., 2018. Detection of prebiotic
845 molecules in plasma and photochemical aerosol analogs using GC/MS/MS techniques.
846 Astrophys. J. 865, 133 (8 pp). https://doi.org/10.3847/1538-4357/aadba1
847 Sekine, Y., Imanaka, H., Matsui, T., Khare, B.N., Bakes, E.L.O., McKay, C.P., Sugita, S., 2008.
848 The role of organic haze in Titan's atmospheric chemistry: I. Laboratory investigation on
849 heterogeneous reaction of atomic hydrogen with Titan tholin. Icarus 194, 186–200.
850 https://doi.org/10.1016/j.icarus.2007.08.031
851 Sham, T.K., Yang, B.X., Kirz, J., Tse, J.S., 1989. K-Edge near-edge X-ray absorption fine
852 structure of oxygen and carbon-containing molecules in the gas phase. Phys. Rev. A 40, 652–
853 669. https://doi.org/10.1103/PhysRevA.40.652
854 Shard, A.G., Whittle, J.D., Beck, A.J., Brookes, P.N., Bullett, N.A., Talib, R.A., Mistry, A., Barton,
855 D., McArthur, S.L. (2004) A NEXAFS examination of unsaturation in plasma polymers of
856 allylamine and propylamine. J. Phys. Chem. B 108, 12472–12480. https://doi.org/10.1021/
857 jp048250f
858 Somogyi, A., Oh, C.-H., Smith, M.A., Lunine, J.I., 2005. Organic environments on Saturn's moon,
859 Titan: Simulating chemical reactions and analyzing products by FT-ICR and ion-trap mass

spectrometry. J. Am. Soc. Mass Spectrom. 16, 850–859. https://doi.org/10.1016/j.jasms.2005.01.027

Stöhr, J., 1992. NEXAFS spectroscopy (corrected ed.), Springer-Verlag, Heidelberg, Germany, pp. 133–137. https://doi.org/10.1007/978-3-662-02853-7

Strobel, D.F., Shemansky, D.E., 1982. EUV emission from Titan's upper atmosphere: Voyager 1 encounter. J. Geophys. Res.: Space Physics 87, 1361–1368. https://doi.org/10.1029/JA087iA03p01361

Szopa, C., Cernogora, G., Boufendi, L., Correia, J.J., Coll, P., 2006. PAMPRE: A dusty plasma experiment for Titan's tholins production and study. Planet. Space Sci. 54, 394–404. https://doi.org/10.1016/j.pss.2005.12.012

Teanby, N.A., Irwin, P.J.G., Nixon, C.A., de Kok, R., Vinatier, S., Coustenis, A., Sefton-Nash, E., Calcutt, S.B., Flasar, F.M., 2012. Active upper-atmosphere chemistry and dynamics from polar circulation reversal on Titan. Nature 491, 732–735. https://doi.org/10.1038/nature11611

Trainer, M.G., Pavlov, A.A., Curtis, D.B., McKay, C.P., Worsnop, D.R., Delia, A.E., Toohey, D.W., Toon, E.B., Tolbert, M.S., 2004. Haze aerosols in the atmosphere of early Earth: Manna from heaven. Astrobiology 4, 409–419. https://doi.org/10.1089/ast.2004.4.409

Tran, B.N., Force, M., Briggs, R.G., Ferris, J.P., Persans, P., Chera, J.J., 2008. Titan's atmospheric chemistry: Photolysis of gas mixtures containing hydrogen cyanide and carbon monoxide at 185 and 254 nm. Icarus 193, 224–232. https://doi.org/10.1016/j.icarus.2007.09.010

Tran, B.N., Joseph, J.C., Ferris, J.P., Persans, P.D., Chera, J.J., 2003. Simulation of Titan haze formation using a photochemical flow reactor: The optical constants of the polymer. Icarus 165, 379–390. https://doi.org/10.1016/S0019-1035(03)00209-4

882 Urquhart, S.G., Ade, H., 2002. Trends in the carbonyl core (C 1S, O 1S) → $\pi^*_{C=O}$ transition in the
883 near-edge X-ray absorption fine structure spectra of organic molecules. J. Phys. Chem. B 106,
884 8531–8538. https://doi.org/10.1021/jp0255379
885 Vinatier, S., Bézard, B., Lebonnois, S., Teanby, N.A., Achterberg, R.K., Gorius, N., Mamoutkine,
886 A., Guandique, E., Jolly, A., Jennings, D.E., Flasar, F.M., 2015. Seasonal variations in Titan's
887 middle atmosphere during the northern spring derived from Cassini/CIRS observations. Icarus
888 250, 95–115. https://doi.org/10.1016/j.icarus.2014.11.019
889 Wilson, E.H., Atreya, S.K., 2003. Chemical sources of haze formation in Titan's atmosphere.
890 Planet. Space Sci. 51, 1017–1033. https://doi.org/10.1016/j.pss.2003.06.003
891 Wirick, S., Flynn, G.J., Keller, L.P., Nakamura-Messenger, K., Peltzer, C., Jacobsen, C., Sandford,
892 S.A., Zolensky, M.E., 2009. Organic matter from comet 81P/Wild 2, IDPs, and carbonaceous
893 meteorites; similarities and differences. Meteorit. Planet. Sci. 44, 1611–1626. https://doi.org/
894 10.1111/j.1945-5100.2009.tb01194.x
895 Zarnecki, J.C., Leese, M.R., Hathi, B., Ball, A.J., Hagermann, A., Towner, M.C., Lorenz, R.D.,
896 McDonnell, J.A.M., Green, S.F., Patel, M.R., Ringrose, T.J., Rosenberg, P.D., Atkinson, K.R.,
897 Paton, M.D., Banaszkiewicz, M., Clark, B.C., Ferri, F., Fulchignoni, M., Ghafoor, N.A.L.,
898 Kargl, G., Svedhem, H., Delderfield, J., Grande, M., Parker, D.J., Challenor, P.G., Geake, J.E.,
899 2005. A soft solid surface on Titan as revealed by the Huygens Surface Science Package.
900 Nature 438, 792–795. https://doi.org/10.1038/nature04211
901 Zhao, T.Q., Li, Q., Liu, B.S., Gover, R.K.E., Sarre, P.J., Cheung, A.S.-C., 2016. Laboratory
902 astrochemistry: catalytic conversion of acetylene to polycyclic aromatic hydrocarbons over
903 SiC grains. Phys. Chem. Chem. Phys. 18, 3489–3496. https://doi.org/10.1039/C5CP06425B

Zhou, J., Zhou, X., Li, R., Sun, X., Ding, Z., Cutler, J., Sham, T.-K., 2009. Electronic structure and luminescence center of blue luminescent carbon nanocrystals. Chem. Phys. Lett. 474, 320–324. https://doi.org/10.1016/j.cplett.2009.04.075

Zhu, Q., Money, S. L., Russell, A. E., Thomas, K. M., 1997. Determination of the fate of nitrogen functionality in carbonaceous materials during pyrolysis and combustion using X-ray absorption near edge structure spectroscopy. Langmuir 13, 2149–2157. https://doi.org/10.1021/la961027s

Table 1

Assignments of the main bands observed at the carbon (C1–C5, Fig. 2) and nitrogen (N1–N3, Fig. 3) 1s edge XANES spectra of all four tholins. A more complete list of possible assignments of all the bands (including minor bands) in these C- and N-XANES spectra are listed in Tables S1 and S2 (Supplementary Material), respectively. The band N2* corresponds to the band N2 that is redshifted in tholins produced from gas mixtures that did not contain acetylene (Fig. 3). C and N atoms involved in their respective XANES bands are marked in bold.

	Band	Energy (eV)	Assignment	Transition	References*
Carbon edge	C1	285.0–285.3	Aromatic **C**=C	1s → π*	1,2,3
	C2	285.7–286.0	Imine **C**=N	1s → π*	4,5
	C3	286.8–287.0	Nitrile **C**≡N	1s → π*	2,4,6,7,8
	C4	287.8–288.3	Amide O=**C**–NH_x	1s → π*	2,9
	C4	287.9–288.2	Benzene [Ar]**C**	1s → π*	10
	C5	288.9–289.2	Amorphous C (sp^3)	1s → 3p/σ*	10
	C5	288.9–289.4	Alcohol **C**H_x–OR	1s → 3p/σ*	11,12,13
	C5	288.9–289.7	Urea group $(NH_x)_2$**C**=O	1s → π*	2
Nitrogen edge	N1	398.2–399.1	Imine C=**N**	1s → π*	2,7,14
	N2*	399.3–399.8	Nitrile (aliphatic) C≡**N**	1s → π*	2,5,14,15,16
	N2	399.8–400.0	Nitrile (aromatic) C≡**N**	1s → π*	17
	N3	401.0–401.3	Amide O=C–**N**H_x	1s → π*	2,3,14,18
	N3	401.0–401.4	Heterocyclic nitrogen	1s → π*	15
	N3	401.1–401.4	Amine C–**N**H_x	1s → 3p/σ*	3

920 *References: **(1)** Stöhr (1992); **(2)** Cody et al. (2008); **(3)** Cody et al. (2011); **(4)** Dhez et al. (2003); **(5)**
921 Shard et al. (2004); **(6)** Kikuma et al. (1998); **(7)** Apen et al. (1993); **(8)** Zhou et al. (2009); **(9)** Urquhart
922 and Ade (2002); **(10)** Díaz et al. (2001); **(11)** Ishii and Hitchcock (1988); **(12)** Sham et al. (1989); **(13)**
923 Lehmann et al. (2005); **(14)** Leinweber et al. (2007); **(15)** Pels et al. (1995); **(16)** Ray et al. (2005); **(17)** Zhu
924 et al. (1997); **(18)** Gordon et al. (2003).
925

926 **Table 2**

927 Elemental C/N ratios determined from fitting the full-range XANES spectra of all tholins spanning
928 the C, N, and O 1s edges (Fig. 4) with the atomic mass absorption coefficients (Henke et al., 1993,
929 see Sections 2.2 and 3.3 for details). Error bars are due to the fitting method used (Cody et al.,
930 2008; Nuevo et al., 2011).

Initial gas mixture	C/N Ratio
N_2:CH_4 (90:10)	0.9 ± 0.3
N_2:CH_4:C_2H_2 (89.5:10:0.5)	2.2 ± 0.4
N_2:CH_4 (95:5)	1.3 ± 0.2
N_2:CH_4:C_2H_2 (94.5:5:0.5)	2.4 ± 0.4

931

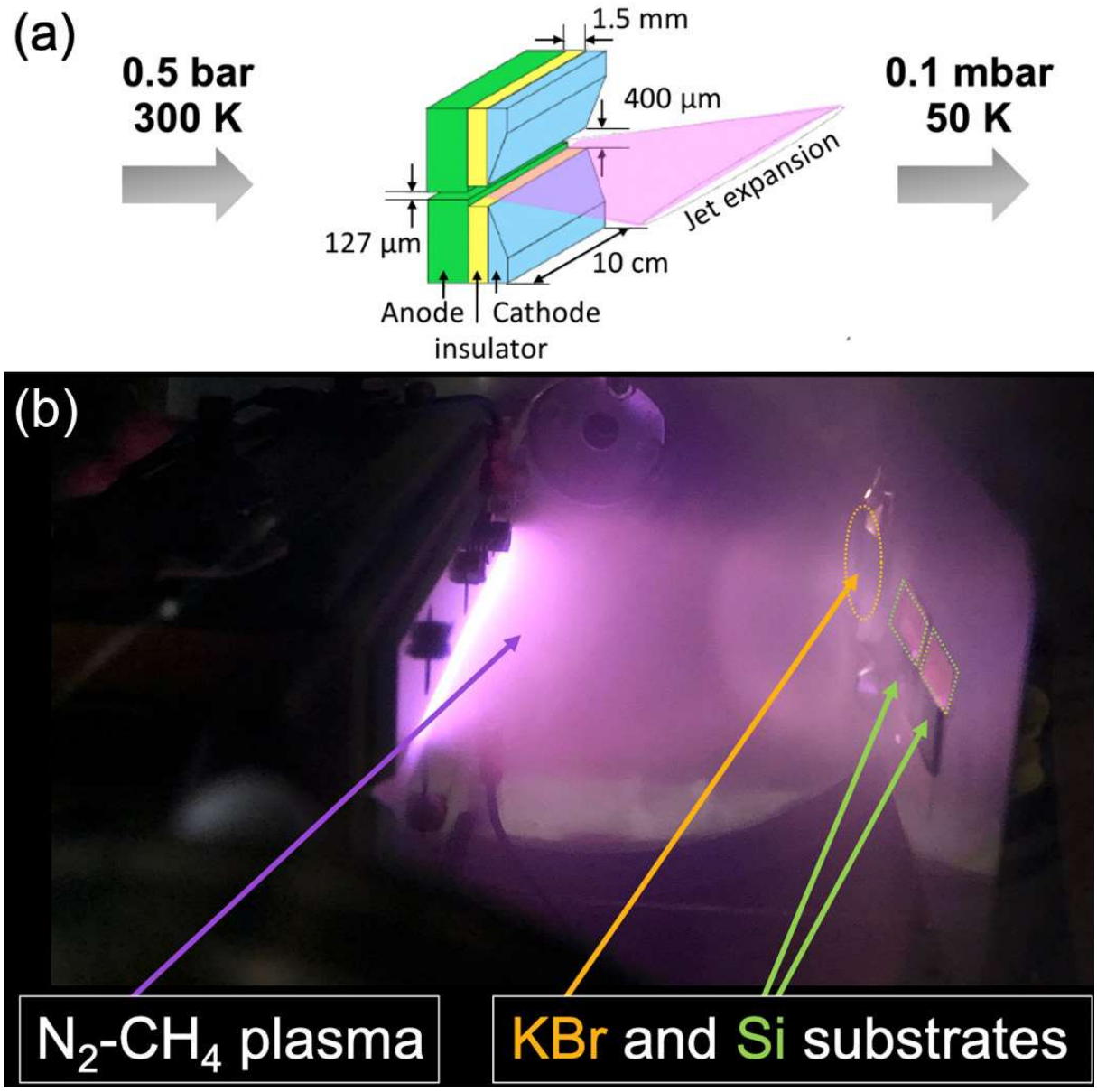

Fig. 1. (a) Schematic of the COSmIC/THS adiabatic expansion of the gas allowing to achieve low temperatures and pressures that are representative of cold atmospheres such as that of Titan (from Broks et al., 2005). The plasma discharge is the energy source used to induce the chemistry in the expansion, by simulating the chemistry induced by charged particles in planetary atmospheres. (b) Actual photograph of the expansion and plasma in the COSmIC/THS chamber, which also shows how the so-formed solid particles ('tholins') are deposited on different substrates. Si_3N_4 substrates were used for the experiments reported here.

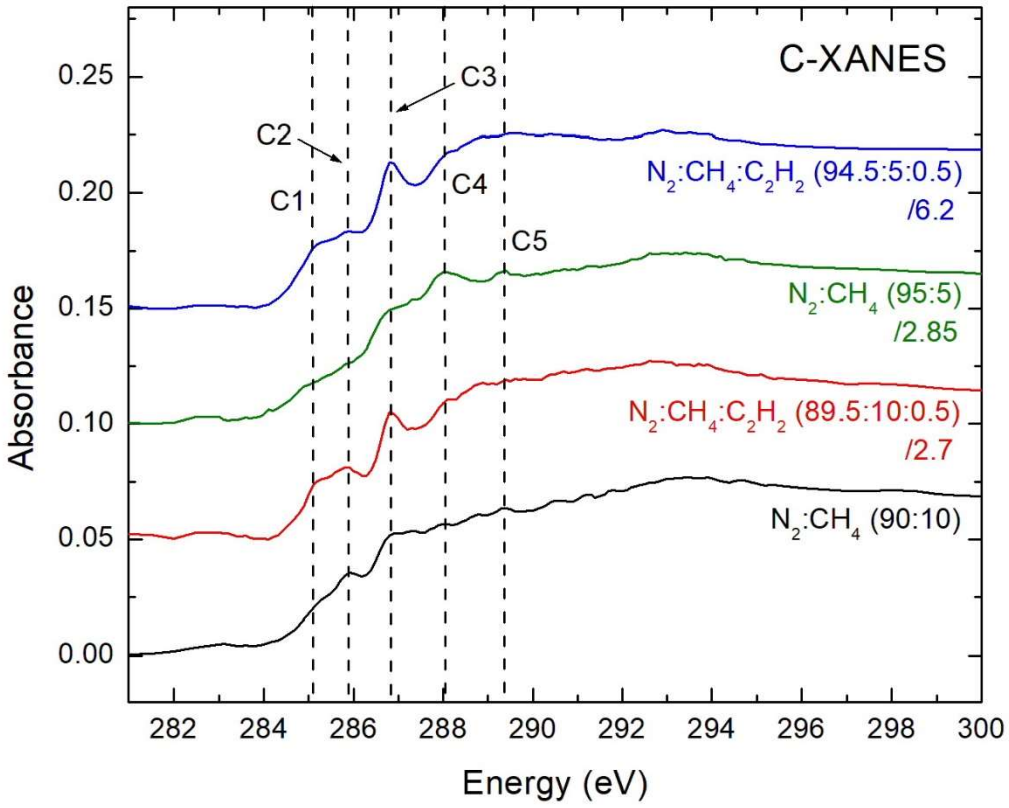

940

941 **Fig. 2.** XANES spectra at the carbon 1s edge of the four tholin samples produced in the present
942 study. **The intensities of the spectra are normalized to the C-edge peak intensity of the N_2:CH_4**
943 **(90:10) spectrum. Normalization factors are provided below each gas mixture composition**
944 **on the plot.** The main bands (C1–C5) are highlighted with dashed lines and their assignments are
945 given in Table 1. Minor bands are listed in Table S1 (Supplementary Material). Absorbances of
946 the spectra are normalized and offset for clarity.

947

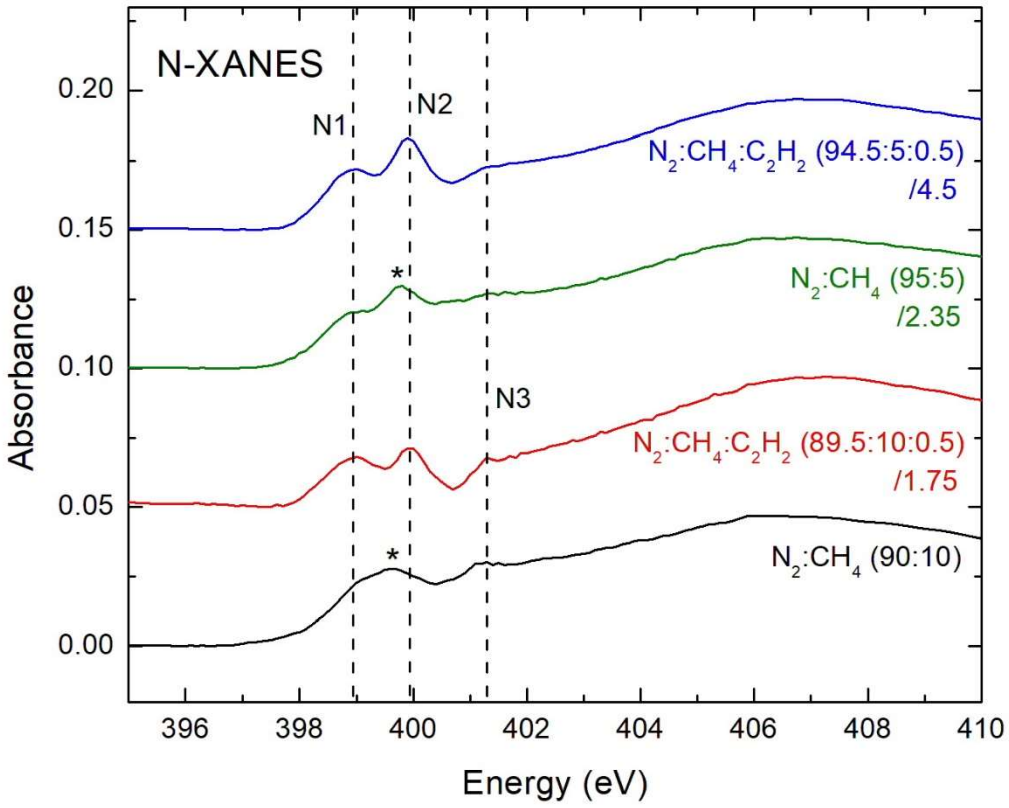

948

949 **Fig. 3.** XANES spectra at the nitrogen 1s edge of the four tholin samples produced in the present
950 study. **The intensities of the spectra are normalized to the N-edge peak intensity of the N_2:CH_4**
951 **(90:10) spectrum. Normalization factors are provided below each gas mixture composition**
952 **on the plot.** The main bands (N1–N3) are highlighted with dashed lines and their assignments are
953 given in Table 1. Minor bands are listed in Table S2 (Supplementary Material). The bands marked
954 with an asterisk correspond to band N2 that is redshifted in energy and referred to as band N2*
955 (Table 1, Section 3.2). Absorbances of the spectra are normalized and offset for clarity.

956

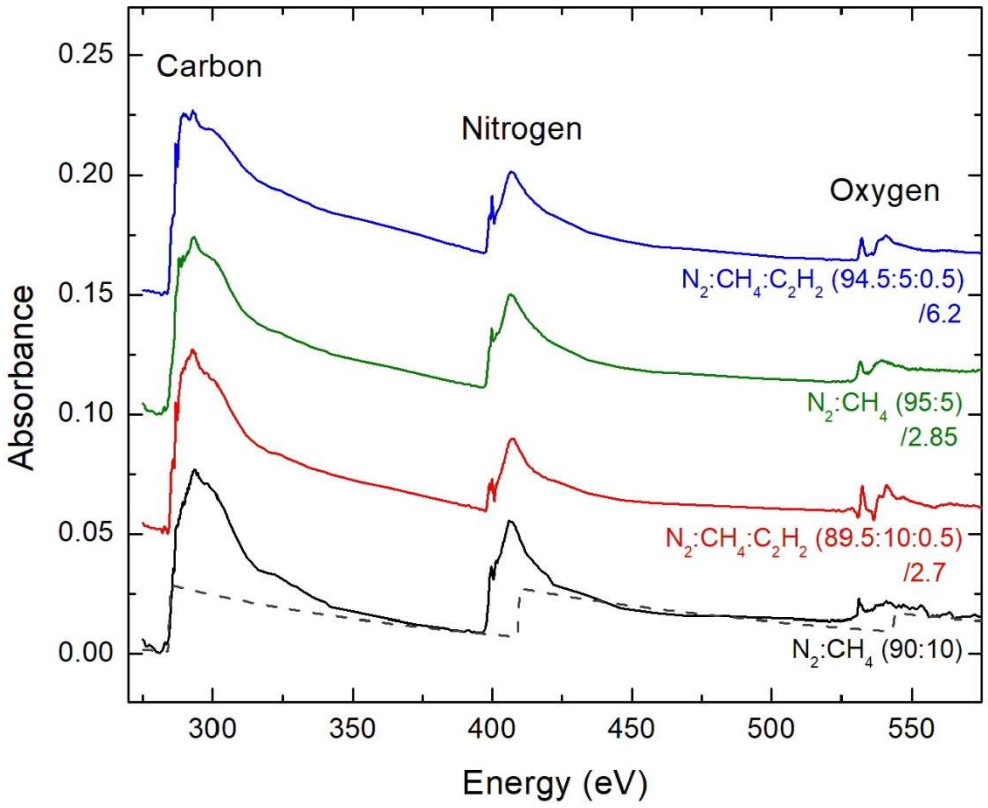

957

958 **Fig. 4.** Full-range XANES spectra spanning the C, N, and O 1s edges (275–575 eV) of the four
959 tholin samples produced in the present study. **The intensities of the spectra are normalized to**
960 **the C-edge peak intensity of the N_2:CH_4 (90:10) spectrum. Normalization factors are**
961 **provided below each gas mixture composition on the plot.** These spectra were used to determine
962 the C/N and C/O ratios of each sample, after fitting the spectra with atomic mass absorption
963 coefficients (see Sections 3.3 and **3.5**, respectively). An example of such computational fit is
964 shown for the spectrum of the tholin produced from the N_2:CH_4 (90:10) gas mixture (dashed grey
965 curve). Detailed XANES spectra at the C and N 1s edges are shown in Figs. 2 and 3, respectively,
966 and the assignments of the bands at the C and N edges are given in Table 1. Detailed XANES
967 oxygen 1s edge spectra are shown in Fig. S1 and the assignments of the bands are given in Tables

968 S1 and S2 (Supplementary Material). Absorbances of the spectra are normalized and offset for
969 clarity.
970

The Titan Haze Simulation (THS) experiment on COSmIC. Part III. XANES study of laboratory analogs of Titan tholins

Michel Nuevo, Ella Sciamma-O'Brien, Scott A. Sandford, Farid Salama, Christopher K. Materese, and A.L. David Kilcoyne

Supplementary Material

Table S1

Complete list of possible assignments of all the main (C1–C5) and minor bands observed at the XANES carbon 1s edge spectra of all tholins (Fig. 2). Bands C1–C5 are the same as those labeled in Fig. 2 and Table 1. Because of the small intensities of the minor bands, their assignments are tentative. Note that assignments do not necessarily indicate the presence of specific compounds; rather, they are indicative of chemical bonds that are consistent with such compounds. C atoms involved in the XANES bands are marked in bold. [Ar], aromatic ring; R, carbon chain.

Band	Energy (eV)	Assignment	Transition	References*
	282.8–283.2	Amorphous C		1,2
	283.5–283.9	*p*-Benzoquinone C=**C**–C=O	1s → π*	3
	284.1–284.3	Quinone C=**C**–C=O	1s → π*	4
		Protonated aromatic [Ar]**C**–H	1s → π*	4
	284.6–284.7	Amorphous C (sp^2)	1s → π*	5,6
	284.9–285.4	Alkylated aromatic [Ar]**C**–R	1s → π*	7,8
		Protonated aromatic [Ar]**C**–H	1s → π*	7,8
C1	285.0–285.3	Aromatic **C**=C	1s → π*	9,10,11
	285.2–285.4	Graphite (C sp^2)	1s → π*	12,13,14,15
C2	285.7–286.0	Imine **C**=N	1s → π*	16,17
	285.7–286.2	Aromatic carbonyl [Ar]–**C**=O	1s → π*	18
	285.8–286.2	Amorphous C	p5	12
		p-Benzoquinone C=**C**–C=O	1s → π*	3
	286.0–286.2	Conjugated ketone C=**C**–C=O	1s → π*	10,11
C3	286.8–287.0	Nitrile **C**≡N	1s → π*	10,15,16,19,20
		Pyridine **C**=N	1s → π*	21
		Ketone **C**=O	1s → π*	4,22,23
	286.8–287.1	Aliphatic C–**C**–H	1s → 3p/σ*	15
	287.0–287.5	Aromatic alcohol [Ar]**C**–OH	1s → π*	3,4
		Aliphatic ketone C–**C**=O	1s → π*	24,25
	287.1–288.0	Enol C=**C**–OH	1s → π*	10
	287.2–288.3	Aliphatic **C**–C	1s → 3p/σ*	10,22,24,26,27
	287.3–287.7	Aliphatic **C**–H	1s → 3p/σ*	11
	287.7–288.3	Aromatic carbonyl [Ar]–**C**=O	1s → π*	18
C4	287.8–288.3	Amide O=**C**–NH_x	1s → π*	10,23
C4	287.9–288.2	Benzene [Ar]**C**	1s → π*	6

	288.0–288.8	Carboxylic acid O=**C**–OH	1s → π*	6,23,24,28
	288.6–289.0	Diamond (C sp^3)	1s → 3p/σ*	12
C5	288.9–289.2	Amorphous C (sp^3)	1s → 3p/σ*	6
C5	288.9–289.4	Alcohol **C**H_x–OR	1s → 3p/σ*	4,24,25
C5	288.9–289.7	Urea group $(NH_x)_2$**C**=O	1s → π*	10
	289.4–289.7	Secondary alcohol R_2**C**H–OH	1s → 3p/σ*	11
	289.5–290.1	Amorphous C (sp^3)	1s → 3p/σ*	6
	290.1	Alkene **C**=C	1s → 3p/σ*	29
		Carbamoyl NH_x(**C**=O)O–R	1s → π*	10
	290.3–294.6	Carbonate R–O(**C**=O)O–R	1s → π*	10,30
	290.4–290.8	Pyridine **C**–N (sp^2)		15
	290.6–290.8	Amorphous C	1s → 3p/σ*	6
		p-Benzoquinone C=**C**–C=O	1s → π*	3
		Fullerene C_{60}	1s → 3p/σ*	31
	291.2–291.9	Graphite **C**–C	1s → 3p/σ*	6
	293.4–293.8	*p*-Benzoquinone C=**C**–C=O	1s → σ*	3
		p-Benzoquinone C=C–**C**=O	1s → π*	3

*References: (1) Gago et al. (2005); (2) Ray et al. (2006); (3) Francis and Hitchcock (1992); (4) Lehmann et al. (2005); (5) Gutiérrez et al. (1995); (6) Díaz et al. (2001); (7) Hitchcock et al. (1987); (8) Robin et al. (1988); (9) Stöhr (1992); (10) Cody et al. (2008); (11) Cody et al. (2011); (12) Jimenez et al. (2003); (13) Ray et al. (2005); (14) Abrasonis et al. (2008); (15) Zhou et al. (2009); (16) Dhez et al. (2003); (17) Shard et al. (2004); (18) Hitchcock et al. (1992); (19) Apen et al. (1993); (20) Kikuma et al. (1998); (21) Bhattacharyya et al. (2000); (22) Hitchcock and Brion (1980); (23) Urquhart and Ade (2002); (24) Ishii and Hitchcock (1988); (25) Sham et al. (1989); (26) Hitchcock et al. (1986); (27) Hitchcock and Ishii (1987); (28) Ishii and Hitchcock (1987); (29) Ziethen et al. (2002); (30) Flynn et al. (1997); (31) Terminello et al. (1991).

Table S2

Complete list of possible assignments of all the main and minor bands observed at the XANES nitrogen 1s edge spectra of all tholins (Fig. 3). Bands N1–N3 are the same as those labeled in Fig. 3 and Table 1. Because of the small intensities of the minor bands, their assignments are tentative. Note that assignments do not necessarily indicate the presence of specific compounds; rather, they are indicative of chemical bonds that are consistent with such compounds. N atoms involved in the XANES bands are marked in bold. [Py], pyridinic ring; R, carbon chain; [Ar], aromatic ring.

Band	Energy (eV)	Assignment	Transition	References*
	398.2–399.0	Pyridine C=**N**	1s → π*	1,2
N1	398.2–399.1	Imine C=**N**	1s → π*	3,4,5
	399.0–399.3	Heterocyclic nitrogen (‘center’)	1s → π*	1
	399.2–399.6	Amine C–**N**H_2	1s → 3p/σ*	1
N2*	399.3–399.8	Nitrile (aliphatic) C≡**N**	1s → π*	1,2,4,5,6
	399.6–399.9	Pyridine amine [Py]–**N**H_2		7,8,9
N2	399.8–400.0	Nitrile (aromatic) C≡**N**	1s → π*	8
	399.9–400.2	Nitroso group C–**N**=O		1
	400.2–400.5	Pyridine		1
	400.2–400.6	Pyrrole		1
	400.5–401.2	Nitrogen in graphene		10
	400.6–400.8	Protonated imine C=**N**H^+	1s → π*	11
	400.6–401.1	Pyridone [**Py**]C=O		1,9
	400.9–401.2	Nitrile (aromatic) C≡**N**	1s → π*	8
	400.9–401.7	Quaternary nitrogen **N**R_4^+		1,8
N3	401.0–401.3	Amide O=C–**N**H_x	1s → π*	4,5,12,13
N3	401.0–401.4	Heterocyclic nitrogen (‘valley’)	1s → π*	1
N3	401.1–401.4	Amine C–**N**H_x	1s → 3p/σ*	12
	401.3–401.6	Nitrile (aliphatic) C≡**N**	1s → π*	8
	401.3–401.7	Nitrogen in graphene		14
	401.4–401.9	Amide (peptide) O=C–**N**HR	1s → π*	4,5,12,13
	401.4–402.1	Pyridone [**Py**]C=O		1,9
	401.6–401.9	Urea group (**N**H_x)$_2$C=O	1s → π*	15
	402.1–402.6	Amine C–**N**H_x	1s → 3p/σ*	5
	402.3–404.0	Pyrrole		7,8,9,12
	402.5–402.8	Oxidized pyrrole		7

402.8–403.2	Urea group ($\mathbf{N}H_x)_2C=O$	1s → π*	5
	Carbazole		7
402.9–403.4	Pyridine *N*-oxide [Py]–$\mathbf{N}^+$–O^-		1,8
403.2–403.5	Porphyrin		7
403.3–403.5	Nitrile C≡**N**	1s → π*	9
	Diacylimide [R–(C=O)]$_2$**N**H		16
403.4–403.5	Pyridone [**Py**]C=O		9
403.4–403.8	Nitro group C–$\mathbf{N}O_2$	1s → π*	12
403.5–404.0	Aromatic nitro group [Ar]–$\mathbf{N}O_2$	1s → π*	4,12,17
403.8–403.9	Pyridine		8
403.8–404.0	Carbazole		8
404.8–405.0	Aromatic amine [Ar]–$\mathbf{N}H_2$	1s → 3p/σ*	7,8
	Pyridine *N*-oxide [Py]–$\mathbf{N}^+$–O^-		8
405.3–405.5	Nitrate $\mathbf{N}O_3^-$	1s → π*	4
405.9–406.2	Nitro group C–$\mathbf{N}O_2$	1s → π*	1
406.0–406.5	Saturated amine $\mathbf{N}R_3$	1s → 3p/σ*	7,8
407.0–407.2	Pyridine	1s → σ*	10
	Nitrogen in graphene	1s → σ*	10
407.4–407.8	Saturated amine $\mathbf{N}R_3$	1s → 3p/σ*	7,8

*References: (1) Pels et al. (1995); (2) Ray et al. (2005); (3) Apen et al. (1993); (4) Leinweber et al. (2007); (5) Cody et al. (2008); (6) Shard et al. (2004); (7) Mitra-Kirtley et al. (1993); (8) Zhu et al. (1997); (9) Xiao et al. (2005); (10) Hellgren et al. (2001); (11) Hennig et al. (1998); (12) Cody et al. (2011); (13) Gordon et al. (2003); (14) Grant et al. (1994); (15) Urquhart et al. (1995); (16) Lessard et al. (2007); (17) Turci et al. (1996).

Table S3

Complete list of possible assignments of all main (O1–O4) and minor bands observed at the XANES oxygen 1s edge spectra of all tholins (Fig. S1). Because of the small intensities of the minor bands, their assignments are tentative. Note that assignments do not necessarily indicate the presence of specific compounds; rather, they are indicative of chemical bonds that are consistent with such compounds. O atoms involved in the XANES bands are marked in bold. [Ar], aromatic ring; PVMK, poly(vinyl methyl ketone); PEAMA, poly(ethylene-*alt*-maleic acid); PAA, poly(acrylic acid); Asp, aspartic acid; Glu, glutamic acid; PVP, poly(4-vinylphenol); PVA, poly(vinyl alcohol); Ser, serine; Thr, threonine; Tyr, tyrosine; Hyp, hydroxyproline.

Band	Energy (eV)	Assignment	Transition	References*
	530.0	*p*-Benzoquinone [Ar]C=**O**	1s → π*	1
		9-Anthraldehyde C=**O**	1s → π*	2
	530.0–530.2	9-Acetylanthracene **O**=C–CH_3	1s → π*	2
		PVMK **O**=C–CH_3	1s → 3p/σ*	2
O1	531.0	Ketone C=**O**	1s → π*	3,4
		Formaldehyde C=**O**	1s → π*	5,6
		Benzaldehyde [Ar]C=**O**	1s → π*	7
		1-Naphthoic acid C=**O**	1s → π*	2
		PEAMA C=**O**	1s → π*	2
		PAA C=**O**	1s → π*	2
O2	531.6	Ethyl benzoate **O**=C–O–C_2H_5	1s → π*	7
O3	532.1–532.2	Amide **O**=C–NH_x	1s → π*	8
	532.1–532.3	Carboxyl O–C=**O**	1s → π*	3,9
		Methyl formate **O**=C–O–CH_3	1s → π*	7
	532.2–532.3	Amino acids O–C=**O**	1s → π*	10
	532.9–533.1	Phthalic anhydride **O**–C=O		2
		1-Naphthoic acid O=C–**O**–H		2
	533.1	*p*-Benzoquinone [Ar]C=**O**	1s → π*	1
	533.5	Benzaldehyde [Ar]C=**O**	1s → 3s/σ*	7
		Terephthalaldehyde C=**O**	1s → 3s/σ*	7
		PAA O=C–**O**–H		2
O4	534.1–534.2	Alcohol H_xC–**O**–H	1s → 3p/σ*	3,11
O4	534.1–534.2	Carbonate C**O₃**	1s → π*	12
		Asp, Glu O=C–**O**–H	1s → π*	10

534.2	Ethyl benzoate **O**=C–O–C_2H_5	1s → 3s/σ*	7
	Ethyl benzoate O=C–**O**–C_2H_5	1s → π*	7
534.7	PVP [Ar]C=**O**		2
534.7–535.0	Enol C=C–**O**–H	1s → 3p/σ*	3
534.9–535.3	Methyl formate **O**=C–O–CH_3	1s → 3s/σ*	7
	Methyl formate O=C–**O**–CH_3	1s → π*	7
535.4–535.6	Formaldehyde C=**O**	1s → 3s/σ*	5,6
536.2	Formaldehyde C=**O**	1s → 3p/σ*	5,6
	Terephthalaldehyde C=**O**	1s → 4p/σ*	7
536.9–537.0	Methyl cellulose		2
	Methyl formate O=C–**O**–CH_3	1s → 3p/σ*	7
	PVA C–**O**–H		2
537.3–537.6	Benzaldehyde [Ar]C=**O**	1s → 5p/σ*	7
	Ethyl benzoate O=C–**O**–C_2H_5	1s → 3p/σ*	7
537.6	Formaldehyde C=**O**	1s → 4p/σ*	5,6
538.2–538.3	*p*-Benzoquinone [Ar]C=**O**	1s → π*	1
538.2–539.3	Ser, Thr, Tyr, Hyp C–**O**–H	1s → σ*	10
540.7–540.9	Ethyl benzoate O=C–**O**–C_2H_5	1s → σ*	7
540.9–541.0	Methyl formate O=C–**O**–CH_3	1s → σ*	7
541.9–548.6	Amino acids O–C=**O**	1s → σ*	10
542.5–542.7	*p*-Benzoquinone [Ar]C=**O**	1s → σ*	1
544.1	Formaldehyde C=**O**	1s → σ*	5,6
	Benzaldehyde [Ar]C=**O**	1s → σ*	7
	Terephthalaldehyde C=**O**	1s → σ*	7
546.1–546.2	Ethyl benzoate **O**=C–O–C_2H_5	1s → σ*	7
546.9–547.2	Methyl formate **O**=C–O–CH_3	1s → σ*	7
553.9–554.1	*p*-Benzoquinone [Ar]C=**O**	1s → σ*	1

*References: (1) Francis and Hitchcock (1992); (2) Kim et al. (2011); (3) Cody et al. (2008); (4) Yabuta et al. (2014); (5) Hitchcock and Brion (1980); (6) Robin et al. (1988); (7) Hitchcock et al. (1992); (8) De Gregorio et al. (2011); (9) Gordon et al. (2003); (10) Frati et al. (2020); (11) Ishii and Hitchcock (1988); (12) Madix et al. (1988).

Table S4

Elemental C/O ratios determined from fitting the full-range XANES spectra of all tholins spanning the C, N, and O 1s edges (Fig. 4) with the atomic mass absorption coefficients (Henke et al., 1993; see Sections 2.2 and 3.3 for details). Error bars are due to the fitting method used (Cody et al., 2008; Nuevo et al., 2011).

Initial gas mixture	C/O Ratio
N_2:CH_4 (90:10)	2.2 ± 0.9
N_2:CH_4:C_2H_2 (89.5:10:0.5)	2.7 ± 0.6
N_2:CH_4 (95:5)	1.9 ± 0.4
N_2:CH_4:C_2H_2 (94.5:5:0.5)	3.3 ± 0.7

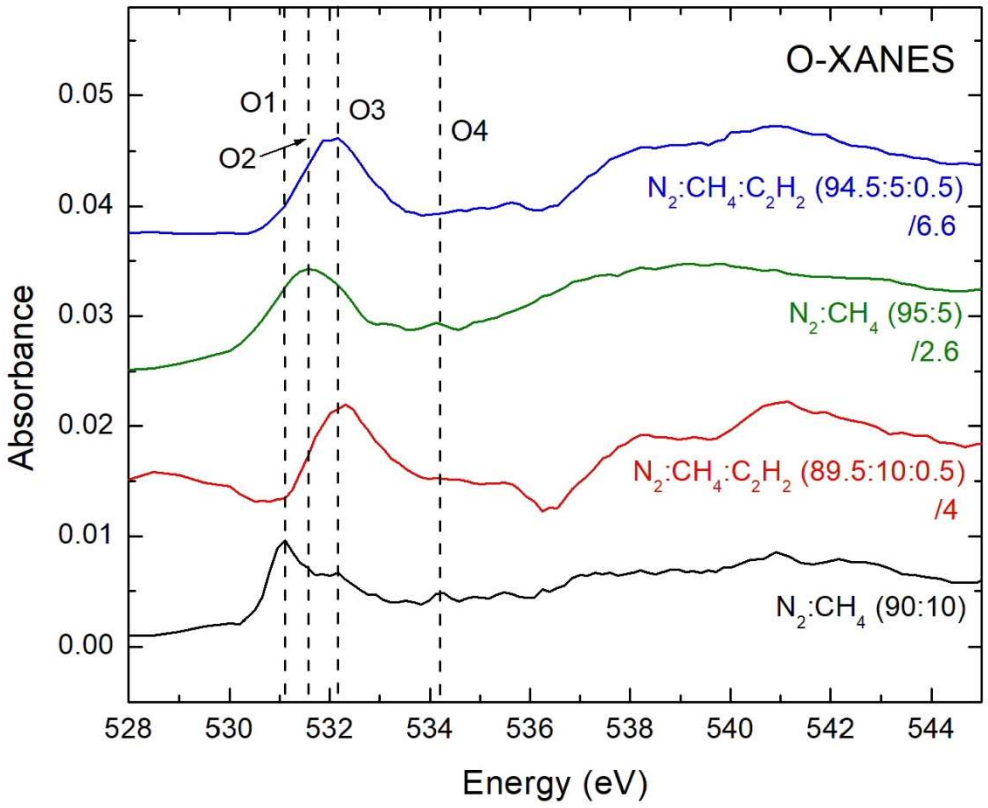

Fig. S1. XANES spectra at the oxygen 1s edge of the four tholin samples produced in the present study. **The intensities of the spectra are normalized to the O-edge peak intensity of the N_2:CH_4 (90:10) spectrum. Normalization factors are provided below each gas mixture composition on the plot.** The main bands (O1–O4) are highlighted with dashed lines and their assignments are given in Table S3, together with the assignments of minor bands. Absorbances of the spectra are normalized and offset for clarity.

Supplementary Material References

Abrasonis, G., Berndt, M., Krause, M., Kuepper, K., Munnik, F., Kolitsch, A., Möller, A., 2008. Soft X-ray absorption and emission spectroscopic investigation of carbon and carbon:transition metal composite films. J. Phys. Chem. C 112, 17161–17170. https://doi.org/10.1021/jp805209r

Apen, E., Hitchcock, A.P., Gland, J.L., 1993. Experimental studies of the core excitation of imidazole, 4,5-dicyanoimidazole, and *s*-triazine. J. Phys. Chem. 97, 6859–6866. https://doi.org/10.1021/j100128a019

Bhattacharyya, S., Lübbe, M., Richter, F., 2000. Near edge x-ray absorption fine structure of thermally annealed amorphous nitrogenated carbon films. J. Appl. Phys. 88, 5043–5049. https://doi.org/10.1063/1.1318389

Cody, G.D., Ade, H., Alexander, C.M.O'D., Araki, T., Butterworth, A., Fleckenstein, H., Flynn, G., Gilles, M.K., Jacobsen, C., Kilcoyne, A.L.D., Messenger, K., Sandford, S.A., Tyliszczak, T., Westphal, A.J., Wirick, S., Yabuta, H., 2008. Quantitative organic and light-element analysis of comet 81P/Wild 2 particles using C-, N-, and O-μ-XANES. Meteorit. Planet. Sci. 43, 353–365. https://doi.org/10.1111/j.1945-5100.2008.tb00627.x

Cody, G.D., Gupta, N.S., Briggs, D.E.G., Kilcoyne, A.L.D., Summons, R.E., Kenig, F., Plotnick, R.E., Scott, A.C., 2011. Molecular signature of chitin-protein complex in Paleozoic arthropods. Geology 39, 255–258. https://doi.org/10.1130/G31648.1

De Gregorio, B.T., Sharp, T.G., Rushdi, A.I., Simoneit, B.R.T., 2011. Bugs or gunk? Nanoscale methods for assessing the biogenicity of ancient microfossils and organic matter. In *Earliest life on Earth: Habitats, environments and methods of detection*, Golding, S., Glikson, M. (Eds.), Springer, Dordrecht, The Netherlands, pp. 239–289. https://doi.org/10.1007/978-90-481-8794-2_10

Dhez, O., Ade, H., Urquhart, S.G., 2003. Calibrated NEXAFS spectra of some common polymers. J. Elec. Spec. Rel. Phenom. 128, 85–96. https://doi.org/10.1016/S0368-2048(02)00237-2

Díaz, J., Anders, S., Zhou, X., Moler, E.J., Kellar, S.A., Hussain, Z., 2001. Analysis of the π* and σ* bands of the x-ray absorption spectrum of amorphous carbon. Phys. Rev. B 64, 125204 (9 pp). https://doi.org/10.1103/PhysRevB.64.125204

Flynn, G.J., Keller, L.P., Kirz, J., Wirick, S., Bajt, S., Chapman, H.N., 1997. Carbon mapping and carbon-XANES measurements on carbonate globules from AH84001. Lunar and Planetary Science Conference XXVIII, 17–21 March 1997, Houston, TX, USA, Abstract No. 1548.

Francis, J.T., Hitchcock, A.P., 1992. Inner-shell spectroscopy of *p*-benzoquinone, hydroquinone, and phenol: Distinguishing quinoid and benzenoid structures. J. Phys. Chem. 96, 6598–6610. https://doi.org/10.1021/j100195a018

Frati, F., Hunault, M.O.J.Y., de Groot, F.M.F., 2020. Oxygen K-edge X-ray absorption spectra. Chem. Rev. 120, 4056–4110. https://doi.org/10.1021/acs.chemrev.9b00439

Gago, R., Vinnichenko, M., Jäger, H.U., Belov, A.Y., Jiménez, I., Huang, N., Sun, H., Maitz, M.F., 2005. Evolution of sp^2 networks with substrate temperature in amorphous carbon films: Experiment and theory. Phys. Rev. B 72, 014120 (9 pp). https://doi.org/10.1103/PhysRevB.72.014120

Gordon, M.L., Cooper, G., Morin, C., Araki, T., Turci, C.C., Kaznatcheev, K., Hitchcock, A.P., 2003. Inner-shell excitation spectroscopy of the peptide bond: Comparison of the C 1*s*, N 1*s*, and O 1*s* spectra of glycine, glycyl–glycine, and glycyl–glycyl–glycine. J. Phys. Chem. A 107, 6144–6159. https://doi.org/10.1021/jp0344390

Grant, K.A., Zhu, Q., Thomas, K.M., 1994. Nitrogen release in the gasification of carbons. Carbon 32, 883–895. https://doi.org/10.1016/0008-6223(94)90045-0

Gutiérrez, A., Díaz, J., López, M.F., 1995. X-ray absorption spectroscopy study of pulsed-laser-evaporated amorphous carbon films. Appl. Phys. A 61, 111–114. https://doi.org/10.1007/BF01538374

Hellgren, N., Guo, J., Såthe, C., Agui, A., Nordgren, J., Luo, Y., Ågren, H., Sundgren, I.E., 2001. Nitrogen bonding structure in carbon nitride thin films studied by soft x-ray spectroscopy. Appl. Phys. Lett. 79, 4348–4350. https://doi.org/10.1063/1.1428108

Henke, B.L., Gullikson, E.M., Davis, J.C., 1993. X-ray interactions: Photoabsorption, scattering, transmission, and reflection at E = 50–30,000 eV, Z = 1–92. Atom. Data Nucl. Data Tab. 54, 181–342. https://doi.org/10.1006/adnd.1993.1013

Hennig, C., Hallmeier, K.H., Szargan, R., 1998. XANES investigation of chemical states of nitrogen in polyaniline. Synthetic Metals 92, 161–166. https://doi.org/10.1016/S0379-6779(98)80106-9

Hitchcock, A.P., Brion, C.E., 1980. Inner-shell excitation of formaldehyde, acetaldehyde and acetone studied by electron impact. J. Elec. Spec. Rel. Phenom. 19, 231–250. https://doi.org/10.1016/0368-2048(80)87006-X

Hitchcock, A.P., Fischer, P., Gedanken, A., Robin, M.B., 1987. Antibonding σ* valence MOs in the inner shell and outer shell spectra of the fluorobenzenes. J. Phys. Chem. 91, 531–540. https://doi.org/10.1021/j100287a009

Hitchcock, A.P., Ishii, I., 1987. Carbon K-shell excitation spectra of linear and branched alkanes. J. Elec. Spec. Rel. Phenom. 42, 11–26. https://doi.org/10.1016/0368-2048(87)85002-8

Hitchcock, A.P., Newbury, D.C., Ishii, I., Stöhr, J., Horsley, J.A., Redwing, R.D., Johnson, A.L., Sette, F., 1986. Carbon K-shell excitation of gaseous and condensed cyclic hydrocarbons: C_3H_6, C_4H_8, C_5H_8, C_5H_{10}, C_6H_{10}, C_6H_{12}, and C_8H_8. J. Chem. Phys. 85, 4849–4862. https://doi.org/10.1063/1.451719

Hitchcock, A.P., Urquhart, S.G., Rightor, E.G., 1992. Inner shell spectroscopy of benzaldehyde, terephthalaldehyde, ethyl benzoate, terephthaloyl chloride, and phosgene: Models for core excitation of poly (ethylene terephthalate). J. Phys. Chem. 96, 8736–8750. https://doi.org/10.1021/j100201a015

Ishii, I., Hitchcock, A.P., 1987. A quantitative experimental study of the core excited electronic states of formamide, formic acid, and formyl fluoride. J. Chem. Phys. 87, 830–839. https://doi.org/10.1063/1.453290

Ishii, I., Hitchcock, A.P., 1988. The oscillator strengths for C1*s* and O1*s* excitation of some saturated and unsaturated organic alcohols, acids and esters. J. Elec. Spec. Rel. Phenom. 46, 55–84. https://doi.org/10.1016/0368-2048(88)80005-7

Jiménez, I., Gago, R., Albella, J.M., 2003. Fine structure at the X-ray absorption π* and σ* bands of amorphous carbon. Diam. Relat. Mater. 12, 110–115. https://doi.org/10.1016/S0925-9635(03)00011-6

Kikuma, J., Warwick, T., Shin, H.-J., Zhang, J., Tonner, B.P., 1998. Chemical state analysis of heat-treated polyacrylo-nitrile fiber using soft X-ray spectromicroscopy. J. Elec. Spec. Rel. Phenom. 94, 271–278. https://doi.org/10.1016/S0368-2048(98)00196-0

Kim, K., Zhu, P., Li, N., Ma, X., Chen, Y., 2011. Characterization of oxygen containing functional groups on carbon materials with oxygen K-edge X-ray absorption near edge structure spectroscopy. Carbon 49, 1745–1751. https://doi.org/10.1016/j.carbon.2010.12.060

Lehmann, J., Liang, B., Solomon, D., Lerotic, M., Luizão, F., Kinyangi, J., Schäfer, T., Wirick S., Jacobsen, C., 2005. Near-edge X-ray absorption fine structure (NEXAFS) spectroscopy for mapping nanoscale distribution of organic carbon forms in soil: Application to black carbon particles. Global Biogeochem. Cycles 19, 1013–1025. https://doi.org/10.1029/2004GB002435

Leinweber, P., Kruse, J., Walley, F.L., Gillespie, A., Eckhardt, K.-U., Blyth, R., Regier, T., 2007. Nitrogen K-edge XANES – An overview of reference compounds used to identify 'unknown' organic nitrogen in environmental samples. J. Synchr. Rad. 14, 500–511. https://doi.org/10.1107/S0909049507042513

Lessard, R., Cuny, J., Cooper, G., Hitchcock, A.P., 2007. Inner-shell excitation of gas phase carbonates and α,γ-dicarbonyl compounds. Chem. Phys. 331, 289–303. https://doi.org/10.1016/j.chemphys.2006.10.020

Madix, R.J., Solomon, J.L., Stöhr, J., 1988. The orientation of the carbonate anion on Ag(110). Surf. Sci. 197, L253–L259. https://doi.org/10.1016/0039-6028(88)90624-3

Mitra-Kirtley, S., Mullins, O.C., Branthaver, J.F., Cramer, S.P., 1993. Nitrogen chemistry of kerogens and bitumens from X-ray absorption near-edge structure spectroscopy. Energy & Fuels 7, 1128–1134. https://doi.org/10.1021/ef00042a062

Nuevo, M., Milam, S.N., Sandford, S.A., De Gregorio, B.T., Cody, G.D., Kilcoyne, A.L.D., 2011. XANES analysis of organic residues produced from the UV irradiation of astrophysical ice analogs. Adv. Space Res. 48, 1126–1135. https://doi.org/10.1016/j.asr.2011.05.020

Pels, J.R., Kapteijn, F., Moulijn, J.A., Zhu, Q., Thomas, K.M., 1995. Evolution of nitrogen functionalities in carbonaceous materials during pyrolysis. Carbon 33, 1641–1653. https://doi.org/10.1016/0008-6223(95)00154-6

Ray, S.C., Chiou, J.W., Pong, W.F., Tsai, M.-H., 2006. The electronic properties of nanomaterials elucidated by synchrotron radiation-based spectroscopy. Crit. Rev. Solid Mater. Sci. 31, 91–110. https://doi.org/10.1080/10408430601044775

Ray, S.C., Pao, C.W., Chiou, J.W., Tsai, H.M., Jan, J.C., Pong, W.F., McCann, R., Roy, S.S., Papakonstantinou, P., McLaughlin, J.A., 2005. Electronic properties of *a*-CN_x thin films: An x-ray-absorption and photoemission spectroscopy study. J. Appl. Phys. 98, 033708 (4 pp). https://doi.org/10.1063/1.1994933

Robin, M.B., Ishii, I., McLaren, R., Hitchcock, A.P. (1988) Fluorination effects on the inner shell spectra of unsaturated molecules. J. Elec. Spec. Rel. Phenom. 47, 53–92. https://doi.org/10.1016/0368-2048(88)85005-9

Sham, T.K., Yang, B.X., Kirz, J., Tse, J.S., 1989. K-Edge near-edge X-ray absorption fine structure of oxygen and carbon-containing molecules in the gas phase. Phys. Rev. A 40, 652–669. https://doi.org/10.1103/PhysRevA.40.652

Shard, A.G., Whittle, J.D., Beck, A.J., Brookes, P.N., Bullett, N.A., Talib, R.A., Mistry, A., Barton, D., McArthur, S.L., 2004. A NEXAFS examination of unsaturation in plasma polymers of allylamine and propylamine. J. Phys. Chem. B 108, 12472–12480. https://doi.org/10.1021/jp048250f

Stöhr, J., 1992. NEXAFS spectroscopy (corrected ed.), Springer-Verlag, Heidelberg, Germany, pp. 133–137. https://doi.org/10.1007/978-3-662-02853-7

Terminello, L.J., Shuh, D.K., Himpsel, F.J., Lapiano-Smith, D.A., Stöhr, J., Bethune, D.S., Meijer, G., 1991. Unfilled orbitals of C_{60} and C_{70} from carbon K-shell X-ray absorption fine structure. Chem. Phys. Lett. 182, 491–496. https://doi.org/10.1016/0009-2614(91)90113-N

Turci, C., Urquhart, S.G., Hitchcock, A.P., 1996. Inner-shell excitation spectroscopy of aniline, nitrobenzene, and nitroanilines. Can. J. Chem. 74, 851–869. https://doi.org/10.1139/v96-094

Urquhart, S.G., Ade, H., 2002. Trends in the carbonyl core (C 1S, O 1S) $\rightarrow \pi^*_{C=O}$ transition in the near-edge X-ray absorption fine structure spectra of organic molecules. J. Phys. Chem. B 106, 8531–8538. https://doi.org/10.1021/jp0255379

Urquhart, S.G., Hitchcock, A.P., Priester, R.D., Rightor, E.G., 1995. Analysis of polyurethanes using core excitation spectroscopy. Part II: Inner shell spectra of ether, urea and carbamate model compounds. J. Polym. Sci. B 33, 1603–1620. https://doi.org/10.1002/polb.1995.090331105

Xiao, B., Boudou, J.P., Thomas, K.M., 2005. Reactions of nitrogen and oxygen surface groups in nanoporous carbons under inert and reducing atmospheres. Langmuir 21, 3400–3409. https://doi.org/10.1021/la0472495

Yabuta, H., Uesugi, M., Naraoka, H., Ito, M., Kilcoyne, A.L.D., Sandford, S.A., Kitajima, F., Mita, H., Takano, Y., Yada, T., Karouji, Y., Ishibashi, Y., Okada, T., Abe, M., 2014. X-ray absorption near edge structure spectroscopic study of Hayabusa category 3 carbonaceous particles. Earth, Planets Space 66, 156 (8 pp). https://doi.org/10.1186/s40623-014-0156-0

Zhou, J., Zhou, X., Li, R., Sun, X., Ding, Z., Cutler, J., Sham, T.-K., 2009. Electronic structure and luminescence center of blue luminescent carbon nanocrystals. Chem. Phys. Lett. 474, 320–324. https://doi.org/10.1016/j.cplett.2009.04.075

Zhu, Q., Money, S.L., Russell, A.E., Thomas, K.M., 1997. Determination of the fate of nitrogen functionality in carbonaceous materials during pyrolysis and combustion using X-ray absorption near edge structure spectroscopy. Langmuir 13, 2149–2157. https://doi.org/10.1021/la961027s

Ziethen, C., Wegelin, F., Schönhense, G., Ohr, R., Neuhäuser, M., Hilgers, H., 2002. Soft X-ray photoelectron microscopy used for the characterization of diamond, a-C and CN_x, thin films. Diam. Relat. Mater. 11, 1068–1073. https://doi.org/10.1016/S0925-9635(01)00597-0